(1) THE BL LAC PHENOMENON: X-RAY OBSERVATIONS OF TRANSITION OBJECTS and (2) DETERMINATION OF THE X-RAY SPECTRUM OF A COMPLETE SAMPLE OF FLAT-SPECTRUM RADIO SOURCES

NASA Grant NAG5-1882

Semiannual Report No. 4

For the Period 15 August 1993 through 14 February 1994

Principal Investigator
Dr. Diana M. Worrall

April 1994

Prepared for:

National Aeronautics and Space Administration
Goddard Space Flight Center
Greenbelt, Maryland 20771

Smithsonian Institution
Astrophysical Observatory
Cambridge, Massachusetts 02138

The Smithsonian Astrophysical Observatory
is a member of the
Harvard-Smithsonian Center for Astrophysics

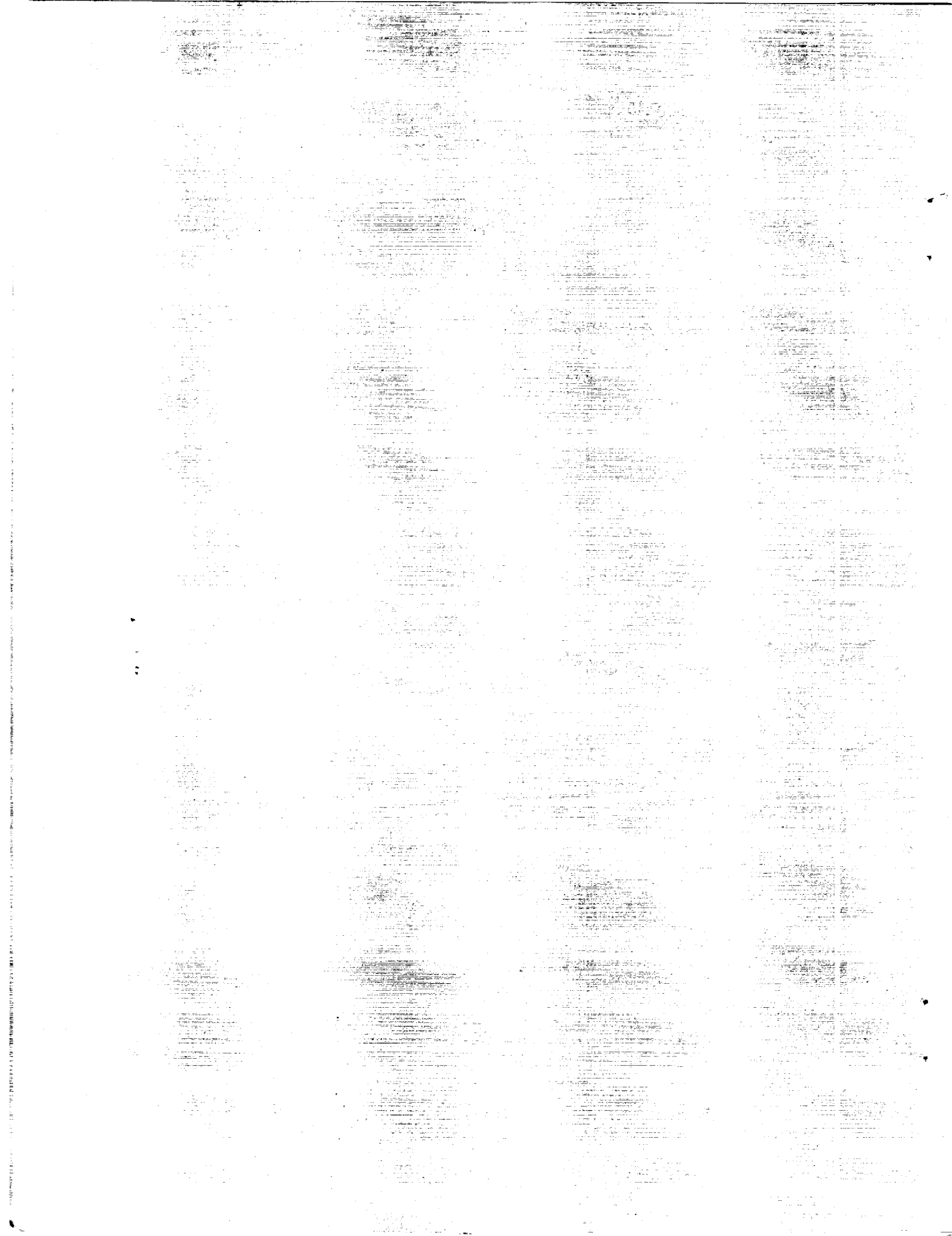

This grant covers two ROSAT investigations. The first, "The BL Lac phenomenon: X-ray observations of transition objects", is an ongoing program to study the X-ray properties of a sample of radio galaxies which are thought to contain BL Lac-type nuclei: new observations were proposed and approved under each ROSAT AO from AO2 onwards. The second, "Determination of the X-ray spectra of a complete sample of flat-spectrum radio sources" is a collaborative program with a group from the University of Tübingen, Germany, where we have successfully competed for ROSAT observing time out of the German time allocation (AO1 through AO3) and Diana Worrall has assisted in planning the program and interpreting the results. AO1 work for this second program was supported by NAG5-1724: AO2 and AO3 work is supported by the subject grant, NAG5-1882.

1 The BL lac phenomenon: X-ray Observations of transition objects

The reporting period saw the acceptance for publication of our first refereed paper on results from this project: "Multiple X-ray Emission Components in Low-Power Radio Galaxies", by D.M. Worrall and M. Birkinshaw, which is to appear in the May 20th 1994 edition of the Astrophysical Journal (see attached preprint). The paper includes spatial and spectral results for 3 radio galaxies observed in AO2 and AO3 specifically for this program, and 3 sources observed as part of a separate ROSAT investigation. A major result is that we have found that both resolved (thermal) and unresolved X-ray emission in a single radio galaxy is typical, although the relative strength and size of the resolved component varies between objects. The unresolved X-ray component correlates well with the core radio emission and may be dominated by non-thermal emission associated with an inner radio jet. In response to comments from the referee we investigated the effects of using a flatter beta model in fitting the resolved thermal emission.

During the reporting period we also began the analysis of ROSAT data for four more radio galaxies observed during AO3 and AO4 as part of this program. Preliminary results suggest that the new data support our earlier conclusions. As we build up results from a sufficiently large sample we will be able to test factors which influence the varied X-ray emission we see.

Several conference presentations of results from the project were also made during the reporting period. This included an oral presentation at the Washington DC AAS meeting, January 1994. Conferences with written proceedings (preprints attached) are

- IAU Symposium 159, "AGN across the Electromagnetic Spectrum" Geneva, September 1993.
- Third annual conference on Astronomical Data Analysis Software and Systems, Victoria BC, October 1993
- ROSAT Science Symposium, Maryland, November 1993

Analysis methods developed for this project were also applied to high-power radio galaxies in collaboration with colleagues from Caltech. During the reporting period a paper

concerning the high-power radio galaxies was accepted for publication in the Astrophysical Journal Letters and it appeared in the January 1st 1994 issue (see attached copy of Worrall et al. paper). During a February 1994 visit of Diana Worrall and Mark Birkinshaw to Caltech, ideas were formed for ROSAT AO5 observing proposals to extend this scientific investigation.

2 Determination of the X-ray spectrum of a complete sample of Flat-spectrum radio sources

This reporting period saw the submission (in December) and acceptance (in February) of a refereed paper which reports the primary results from this project: "X-ray Spectra of a Complete Sample of Extragalactic Core-dominated Radio Sources", by Brunner, Lamer, Worrall, and Staubert, to appear in Astronomy and Astrophysics (copy attached).

The final preparation of the manuscript was assisted by meetings between Diana Worrall and her University of Tübingen collaborators at IAU Symposium 159 in Geneva (September) and the ROSAT Science Symposium in Maryland (November). The referee's comments were minor and our changes in response to them were discussed via electronic mail.

Primary results of the project are that core-dominated radio-loud quasars and BL Lac objects differ in their average ROSAT X-ray spectral index, with the quasars showing the flatter spectrum. The fact that the X-ray spectrum we find for the quasars is flatter than that found for nearby quasars is most easily explained by the existence of soft X-ray emission which is redshifted out of the ROSAT band for quasars at the more typical distances of our sample sources. The results from our project are particularly timely in view of the detection of many core-dominated radio sources (BL Lacs and quasars) in gamma-rays with the EGRET detector on the Compton Gamma Ray Observatory. During the Summer and Fall, pre-publication results from our work were provided to Steve Bloom, a Ph.D. candidate from Boston University, for incorporation in his thesis on the multiwavelength (radio to gamma-ray) emission of core-dominated radio sources.

TO APPEAR IN THE ASTROPHYSICAL JOURNAL, MAY 20TH 1994

MULTIPLE X-RAY EMISSION COMPONENTS IN LOW-POWER RADIO GALAXIES

D.M. WORRALL AND M. BIRKINSHAW
Harvard-Smithsonian Center for Astrophysics, 60 Garden Street, Cambridge, MA 02138
Received *; accepted*

ABSTRACT

We report X-ray observations of the first six sources observed with ROSAT in our study of low-power radio galaxies. Spatial and spectral measurements show that both resolved (thermal) and unresolved X-ray emission in a single source are typical, although the relative strength and size of the resolved component varies between objects. The unresolved X-ray component correlates well with the core radio emission and may be dominated by non-thermal emission associated with an inner radio jet.

Subject headings: galaxies:active – X-rays:galaxies – radio continuum: galaxies – BL Lacertae objects

1. INTRODUCTION

Although the *Einstein* Observatory found that low-power radio galaxies often emit X-rays (Feigelson & Berg 1983; Fabbiano et al. 1984), the dominant physical process responsible for the radiation has remained unclear. Studies of Cen A and M87 have indicated multiple X-ray components (Schreier et al. 1979; Feigelson et al. 1981; Schreier, Gorenstein & Feigelson 1982; Biretta, Stern & Harris 1991) including emission from the active nucleus, jet radiation most likely of synchrotron origin, and diffuse emission probably from hot gas which is now an established constituent of X-ray luminous elliptical galaxies (Forman, Jones & Tucker 1985). The integrated thermal emission from the surrounding Virgo cluster confuses the X-ray emission of M87 (Fabricant & Gorenstein 1983), and for some other low-power radio galaxies a thermal interpretation has been applied to all the X-ray emission (Morganti et al. 1988; Feretti et al. 1990) particularly where the source is resolved or there is known association with a cluster. Correlations have been found between the X-ray emission and both the core and extended radio emission. However, rather than clarifying the situation, these correlations have been used to argue both for a thermal origin (Feigelson & Berg 1983) and a nuclear origin (Fabbiano et al. 1984) for the X-ray emission in radio galaxies.

In this paper we show that a qualitative improvement in radio-galaxy X-ray research is afforded through ROSAT observations. Spatial and spectral measurements show that both resolved (thermal) and unresolved X-ray emission in a single source are typical. For different objects the relative strength of the emissions varies by an order of magnitude, and the linear extent of the gas by a larger factor. The unresolved X-ray component may be dominated by non-thermal emission associated with an inner radio jet.

2. X-RAY OBSERVATIONS & ANALYSIS METHODS

We observed the radio galaxies listed in Table 1 in soft X-rays, at the center of the telescope field of view, with the ROSAT Position-Sensitive Proportional Counter (PSPC; Trümper 1983; Pfeffermann et al. 1987) during the pointed phase of the mission. They are the first sources observed as part of two ongoing programs; one studies a subsample of radio galaxies which Ulrich (1989) proposed are drawn from the parent population of BL Lac objects, and the other is a study of the emission in and around low-power radio galaxies with particularly prominent radio jets.

Table 1: Observations

Object	Name B1950	z	Date	Exposure[a](s)
NGC 315	0055+300	0.0165	1992 Jan 17–Feb 1	10,343
			1992 Jul 19–21	17,869
NGC 326	0055+265	0.047	1992 Jul 24–29	20,969
4C 35.03	0206+355	0.0375	1992 Jul 24–27	14,843
NGC 2484	0755+379	0.0413	1991 Oct 30–Nov 1	15,172
NGC 4261	1216+061	0.0073	1991 Dec 24–30	22,042
NGC 6251	1637+826	0.024	1991 Mar 13–16	14,830

a. Time used in analysis. In some cases intervals of high background have been excluded.

The data we received had already been corrected for instrumental effects and motion of the satellite. For further analysis we used the Post Reduction Off-line Software (PROS; Worrall et al. 1992) and additional software which we developed to convolve the energy-dependent PSPC point response function (PRF; Hasinger et al. 1992) with radially-symmetric spatial models. Only counts within the energy band for which the PRF is well modeled (0.2 – 1.9 keV) are used in the analyses presented in this paper. Some of the data were filtered to remove times of high particle background, and, in some cases, regions around one or more faint contaminating sources were excluded from the analysis. We extracted a background-subtracted radial profile about the maximum-likelihood centroid of X-ray emission for each radio galaxy, and determined the spectral distribution of the counts in the profile. The radial profiles were typically extracted to a radius of 5′.7, with

background from an annulus of radii 3′ to 5′.7 (see Fig. 1, where dotted curves mark the background annuli). The PSPC PRF ($\sim$ 25″ FWHM) is such that the analysis is sensitive to resolved components with radii in the range 3–60 kpc for the nearest galaxy, and 20–380 kpc for the most distant one. NGC 326 is the only source to show obvious asymmetric extended emission; the radial-profile analysis is presented here only to provide a qualitative comparison with the other sources. Its extension is largest towards the NE; we have used only data between position angles 125° and 290° in order to characterize the minimum extent of the emission.

Best fits were determined for each radial profile to an unresolved component, a β model which is appropriate for gas in hydrostatic equilibrium (Cavaliere & Fusco-Femiano 1978; Sarazin 1986), and a combination of an unresolved component and a β model. Results in the tables are for $\beta = 2/3$, which is close to values fit for cluster gas (see e.g., Sarazin 1986), whereas $\beta = 1/2$ may be more typical for gas confined within nearby elliptical galaxies (Forman et al. 1985). Our choice is partly driven by the fact that $\beta \leq 1/2$ gives an infinite X-ray flux so that an extra parameter (a cut-off radius) must be introduced into the models. In the present work we have not attempted to fit values of β from the slope of the power-law region of the model. Indeed, Figure 1 shows that only for the two least extended sources is there any possibility of doing this. Preliminary results give a preference for $\beta = 1/2$ for NGC 4261 and $\beta = 2/3$ for NGC 315. For the other four sources, the measured HWHM (half width half maximum) of the resolved X-ray emission is independent of the value assumed for β. Since

$$\mathrm{HWHM} \propto \theta_{cx}\sqrt{\left(2^{\frac{2}{6\beta-1}}-1\right)} \quad ,$$

we find $\theta_{cx}(\beta = 1/2) = 0.77\theta_{cx}(\beta = 2/3)$; this factor can be applied to the values in Table 2 to calculate $\theta_{cx}(\beta = 1/2)$ for the most extended sources. For small X-ray extensions (NGC 4261 and NGC 315), a decreased β again suggests a smaller core radius, but the observations are sensitive only to the power-law wings of the β model and cannot constrain the core radius. The values in Table 2 should be treated as upper limits to θ_{cx} for NGC 4261 and NGC 315 for values of $\beta < 2/3$.

The counts in each background region contain a contribution from the outer part of the source emission. For all cases except NGC 326 (see §6) the modeled source emission in the background annulus is $\leq 8\%$ of the counts in that annulus. This is small compared with the statistical errors in our radial profiles (see error bars in Fig. 1, and note that for the source with the smallest errors, NGC 4261, the contribution is 2%), and a correction for this emission is made in our model fitting. Each spatial model assumed an energy weighting which is the same as that in the total radial profile.

Our spectral fitting uses the latest versions of the PSPC response-matrix (no. 36) and effective-area (no. 2_6) calibrations. Best fits were determined for each observation to a power law, a thermal model (Raymond & Smith 1977) with 100% cosmic abundances, and a combination of the two.

Since ROSAT data currently have absolute positional uncertainties as large as 10″ over timescales of months (MPE 1992), and to provide an indication of systematic uncertainties in derived model-dependent quantities, we have analyzed separately the two observations of NGC 315 which were 6 months apart (Table 1).

A Friedmann cosmological model with $H_o = 50$ km s^{-1} Mpc^{-1}, $q_o = 0$, is used throughout this paper.

3. RESULTS OF SPATIAL ANALYSIS

The minimum χ^2 values for the three models fit to the radial profiles are given in Table 2. Only NGC 6251 fits unresolved emission acceptably. In all cases a better fit is obtained with an extended β model. However, the addition of an unresolved component to the β model gives a still smaller χ^2 and is $> 99\%$ significant, according to the F test, for all sources except NGC 315, for which the β component is barely resolved (core radius $\theta_{cx} < 20''$) and component separation is difficult with the PSPC. Figure 1 shows the radial profiles and best-fit two-component models, and, like Table 2, is in order of increasing intrinsic core-radius, r_{cx}, of the β-model.

To check that systematic errors in the aspect determination have a negligible effect on our results, we applied our analysis to two BL Lac objects and two quasars spanning similar exposure times and net counts to the radio galaxies; all fitted an unresolved component and excluded the presence of additional resolved X-ray emission of similar strength to that detected in the radio galaxies. The strongest constraint on systematic errors is provided by one of the quasars which has a longer exposure (24 ks) than any of the radio galaxies, and has net counts comparable to the median for the radio galaxies.

Table 2: Radial-profile Model Fits

Object	Unresolved	β-model		β+unresolved		
	component χ^2/dof	χ^2/dof	θ''_{cx}	χ^2/dof	θ''_{cx}	r_{cx} kpc[b]
NGC 4261	436/45	79/44	7	54.4/43	21 ± 5	4
NGC 315[a]	117/45	56/44	4	51.3/43	17 ± 11	8
...	164/45	46/44	5	43.4/43	9 ± 5	4
4C 35.03	325/16	36/15	25	8.2/14	70 ± 15	72
NGC 6251	52/45	43/44	1	25.3/43	130 ± 45	88
NGC 2484	118/16	35/15	3	12.5/14	110 ± 30	124
NGC 326[c]	2928/16	54/15	200	22.0/14	230 ± 30	294

$\beta = 2/3$ assumed in all fits in this Table (see §2).
a. First and second exposures (Table 1) listed separately.
b. Fractional error same as in θ_{cx}. Errors are 1σ.
c. X-ray emission very extended and not radially symmetric. Results for this source should be taken to be qualitative rather than quantitative.

4. RESULTS OF SPECTRAL ANALYSIS

The same net counts which give the radial profiles of Figure 1 are used for our spectral fitting. The presence of a resolved X-ray component in or around each galaxy suggests that at least some of the emission is thermal.

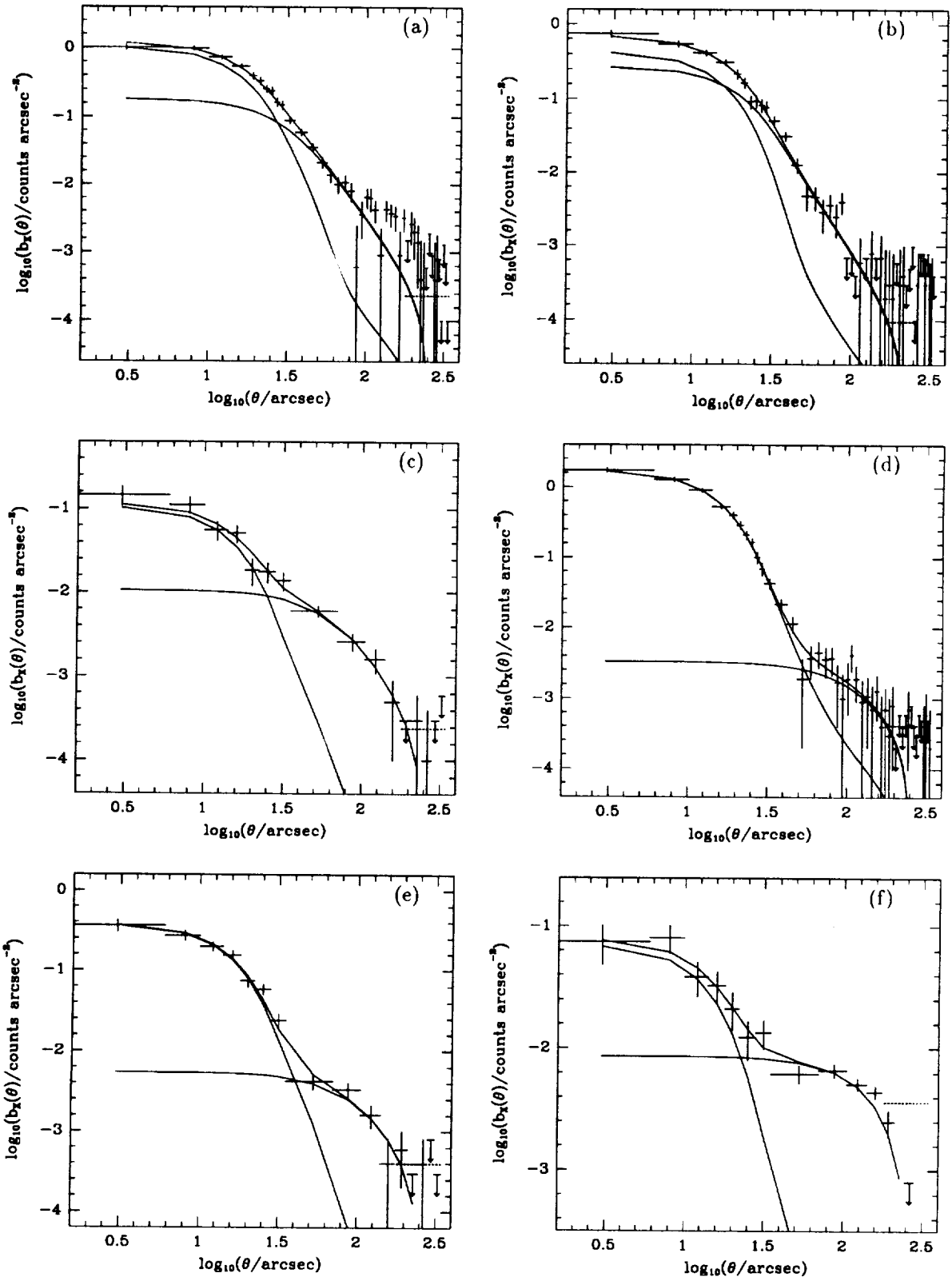

Figure 1. Background-subtracted X-ray radial profiles for radio galaxies in order of increasing intrinsic core-radius of the β model. (a) NGC 4261, (b) NGC 315, second exposure, (c) 4C 35.03, (d) NGC 6251, (e) NGC 2484, and (f) NGC 326. In all cases a combination of point source (narrow curve) and extended β model (broad curve) gives a better fit than either component alone (Table 2). The dotted curve shows the contribution, taken into account in the fitting, of the model to the background annulus.

However, although the fits to a thermal spectrum are in most cases acceptable, in all cases the fit to a power law is better (Table 3). Since a power law is an unlikely model for extended emission of group or cluster dimension, a model which includes at least some thermal emission is suggested. We find similar, improved, and acceptable fits for either a combination of two temperatures or, as given in Table 3, a thermal plus a power law.

For the thermal plus power-law fit, the gas temperatures are similar for all sources except NGC 326, whose spectral parameters are subject to additional systematic uncertainty (see Table 3) and whose dominant resolved emission is of cluster dimension and quite plausibly hotter than 1 keV. When fit to two thermal components, most of the emission from NGC 326 is still from a hot gas of similar > 1 keV temperature, with the counts previously in a soft power law being fit by very soft thermal emission. When the other sources are fit to two thermal components, one is on average about 0.2 keV cooler than that given in Table 3; the other thermal component is generally more poorly constrained and of temperature > 1 keV.

None of the two-component spectral fits or single-temperature thermal fits requires absorption in excess of that from our Galaxy as determined using Stark et al. (1992). Only the unlikely single-component power law requires excess absorption to produce the spectral decrease which is measured in the lowest-energy channels; such a decrease is an intrinsic feature of the low-temperature thermal components.

5. COMPOSITE RESULTS

Our spatial analysis found unresolved emission in all the galaxies, and additional resolved emission of galaxy dimension in the two nearest. To assess the possible contribution from the integrated emission of discrete X-ray sources similar to those in spiral galaxies, we have used the B_0^T magnitudes from deVaucouleurs et al. (1991) and extrapolated 0.2 - 3.5 keV X-ray luminosities of components in our spectral fits for a comparison with the X-ray and optical luminosity correlation for spiral galaxies given in Figure 5 of Fabbiano, Gioia & Trinchieri (1989). The X-ray luminosities of all the separate spectral components for the radio galaxies lie at least an order of magnitude above the corresponding X-ray luminosity in the spiral-galaxy correlation, and are comparable with or exceed 10^{34} W (the limiting X-ray luminosity of spiral galaxies). This argument applies to separate components in both the combined thermal fit and the thermal plus power-law fit, and it leaves hot gas as the most likely explanation for the bulk of the emission from any component which fits a thermal spectrum.

Table 3: Spectral Model Fits

Object	log $N_{H_{Gal}}$	Net cts	Power Law χ^2/dof	Thermal χ^2/dof	Thermal + Power Law χ^2/dof	kT[d] keV	α[d]	log $N_{H_{int}}$[g]	L_{Th} .2–1.9 keV W	L_{PL}[e] .2–1.9 keV W
NGC 4261	20.20	1890 ± 106	26.3/21[c]	30.4/22	2.9/20	$0.6(+0.1,-0.1)$	$0.7(+0.2,-0.2)$	< 20.6	1×10^{34}	1×10^{34}
NGC 315[a]	20.76	528 ± 51	14.5/21[c]	26.4/22	9.5/20	$0.5(+0.2,-0.2)$	$0.9(+0.5,-0.9)$	< 21.7	4×10^{34}	7×10^{34}
...	20.76	858 ± 66	13.2/21[c]	30.6/22	10.6/20	$0.6(+0.1,-0.2)$	$0.8(+0.4,-0.6)$	< 22.0	4×10^{34}	6×10^{34}
4C 35.03	20.77	305 ± 54	6.9/22	7.1/22	5.7/20	$0.8(+0.8,-0.6)$	$-0.5(+1.6,-1.5)$	< 22.4	6×10^{34}	9×10^{34}
NGC 6251[b]	20.74	1540 ± 78	10.3/21[c]	17.3/22	8.8/20	$0.6(+0.3,-0.3)$[b]	$0.4(+0.2,-0.4)$[b]	< 21.9	8×10^{34}	3×10^{35}
NGC 2484	20.70	523 ± 67	5.1/21[c]	12.3/22	5.2/20	$0.7(+0.4,-0.5)$	$1.4(+0.5,-0.7)$	< 21.8	8×10^{34}	4×10^{35}
NGC 326[f]	20.74	1401 ± 42[f]	51.6/22	146.0/22	20.0/20	$3.0(+1.6,-1.0)$[f]	$3.3(+0.6,-0.4)$[f]	< 20.4	7×10^{35}	9×10^{35}

a. First and second exposures (Table 1) listed separately.
b. Consistent but better-constrained spectral results for a broader ROSAT energy band are given by Birkinshaw & Worrall (1993).
c. χ^2 reduces by more than unity for inclusion of intrinsic absorption. For the other fits this is not true and we include only Galactic absorption.
d. Errors are 1σ for one interesting parameter, allowing the other parameters to vary.
e. Assuming isotropic emission over 4π, but note that emission may be anisotropic.
f. Net counts adjusted roughly for large model contribution in background region. An additional systematic uncertainty should be applied to the spectral parameters, which should not be used quantitatively (see §6).
g. 3σ upper limits for one interesting parameter, allowing the other parameters to vary.

Although the X-ray data alone do not rule out a thermal origin for the entire X-ray emission that the PSPC measures, there is a reason for considering this unlikely. In the nearest two galaxies, all the emission under discussion (including the hotter, > 1 keV, component) is of galaxy dimension, and for NGC 6251 and NGC 2484 the hot spectral component must be related to the unresolved spatial component (within the galaxy) since these components dominate the counts in their respective analyses. Gas capable of producing this hot spectral component would be unlikely to be retained within the potential wells of these galaxies: the temperatures are more characteristic of the gas in a massive group of galaxies. NGC 6251 provides the largest number of counts and thus the best-constrained temperature for a hot component. In Birkinshaw & Worrall (1993), we have already presented these spectra in detail and argued that, even taking into account the companion galaxies to NGC 6251, there is no plausible site at which the hot component in a two-temperature fit to the data can be confined. From this and other self-consistency arguments we are led to prefer a power-law plus thermal interpretation for the source. NGC 326 is different from the other galaxies presented here in that the resolved asymmetric emission is of cluster dimension, so that a smaller X-ray contribution from unresolved cooler gas is quite plausible.

Table 4: Percentage of Counts in Unresolved Power Law

Object	Spatial Fitting[a]	Spectral Fitting[a]
NGC 4261	51 ± 4	52 ± 6
NGC 315[b]	61 ± 7	57 ± 9
...	41 ± 5	54 ± 7
4C 35.03	29 ± 6	52 ± 15
NGC 6251	93 ± 5	78 ± 6
NGC 2484	65 ± 9	76 ± 15
NGC 326	10 ± 2	25 ± 2

a. 1σ statistical errors for best-fit model. Errors due to uncertainties in the model parameters are not included.
b. First and second exposures (Table 1) listed separately.

Thermal plus power-law fits provide a natural interpretation that the power-law is from the active core of the galaxy, and the < 1 keV temperatures (Table 3) are very reasonable for gas associated with an elliptical galaxy or small group. To test this, Table 4 compares the fractions of counts in the unresolved component derived from the spatial fitting with the fraction of counts in the power law from the spectral fitting. The agreement is particularly good considering that the errors quoted are statistical only and do not include uncertainties in the model parameters, and the spatial analysis did not take into account the different spectral distributions of the β model and the unresolved component. The discrepancy is largest for NGC 326, but this is not surprising given the inadequacies of the current analysis for this obviously complex X-ray-emitting region. NGC 6251 is noteworthy as the only source where the spectral fitting gives significantly fewer counts in the power law than the spatial fitting gives in the unresolved emission. Birkinshaw & Worrall (1993) analyze the central emission in more detail and interpret the unresolved component as non-thermal emission mixed with a small amount of thermal emission from X-ray gas in a cooling flow (cf §7: a longer cooling time is found for the large-scale thermal component).

The remaining discussion will adopt the interpretation of the X-rays from these galaxies as unresolved emission with a predominantly power-law spectrum from the active core of the galaxy combined with resolved emission from a thermal gas. Meanwhile, we await approved observations of four of these galaxies with the ROSAT HRI to search for resolved components on spatial scales as small as $\sim 5''$ to test whether some fraction of the emission unresolved with the PSPC might not instead arise from thermal gas.

6. NOTES ON INDIVIDUAL SOURCES

Further results for individual sources will be presented in forthcoming papers. However, notes on two follow here:

NGC 4261: The 3σ upper limit for intrinsic N_H in the two-component (power-law plus thermal) spectral fit is 4×10^{20} atoms cm^{-2}. This is $\sim$ 10 times smaller than the value inferred from CO absorption (Jaffe & McNamara 1993) against the mm-emission from the nuclear radio source. Such a large difference between the H_2 absorbing column and the inferred X-ray absorbing column is unexpected and requires explanation. If a large fraction of the unresolved X-ray emission from NGC 4261 originates from the same region in the nucleus that produces the mm-wave emission, then one possibility is that the mean X-ray and mm-wave lines of sight to that emission differ. This could arise because of extreme clumping in the molecular material if the detailed X-ray and mm-wave structures of the nucleus are different. Alternatively, the X-rays could emerge from the nucleus along a hole in a dense molecular torus, and be scattered towards the observer by circumnuclear plasma, while the mm-wave radiation takes a direct path through the torus: such a model has been used for NGC 1068 (Elvis & Lawrence 1988). Another possibility is that the excitation temperature of the molecular gas and the CO/H_2 abundance might be substantially different from those in our Galaxy, so that the H_2 column has been overestimated. Finally, it is possible that the X-ray spectrum of NGC 4261 contains a strong soft component that is absorbed in our data by the H_2 column implied by the CO absorption — but then the strength of that soft component and the column density in H_2 are required to be in coincidental balance. Further work on the X-ray and radio data are needed to make progress in testing these possibilities: optical spectropolarimetry of the nucleus of the galaxy would also be helpful.

NGC 326: Obvious large-scale asymmetric X-ray emission is found. The results presented here for this source are qualitative only, since radial symmetry is not an adequate spatial representation, and the spectral and spatial analyses incorporated only approximate adjustments for the large model contribution in the background region (see §2). In view of this structure (to be discussed elsewhere) the errors in Table 3 are likely to be grossly underestimated.

7. THE THERMAL COMPONENT

Table 5 gives the mean cooling time for gas within r_{cx}, using equations 10 and 25 of Birkinshaw & Worrall (1993) and the spatial and spectral parameters derived from our two-component (power-law plus thermal) fits. Only for NGC 4261 and NGC 315, where the hot gas is of galaxy rather than cluster dimensions (see Table 2), is the cooling time short enough that a cooling flow may have begun. For NGC 6251 we have argued elsewhere (Birkinshaw & Worrall 1993, and see §5) that the spectral results support a small thermal contribution to the unresolved emission and that this gas, which is in a cooling flow, provides infalling energy which can power the active nucleus. It remains possible for the other sources that some or all of the unresolved emission is thermal and in a cooling flow, and forthcoming ROSAT HRI observations will test this possibility through improved spatial resolution (see discussion in §5).

Table 5: Gas Cooling Time

Object	$t_{\rm cool}$ within core radius (yr)[b]
NGC 4261	3.4×10^9
NGC 315[a]	4.0×10^9
...	1.4×10^9
4C 35.03	5.2×10^{10}
NGC 6251	1.0×10^{11}
NGC 2484	9.8×10^{10}
NGC 326	1.2×10^{11}

a. First and second exposures (Table 1) listed separately.
b. Uncertainties indicated by the difference between the two results for NGC 315. Weak dependence on Hubble constant; $t_{\rm cool} \propto 1/\sqrt{H_o}$. Value should be compared with the Hubble time, which is $\sim 2 \times 10^{10}\ (H_o/50\ {\rm km\ s^{-1} Mpc^{-1}})^{-1}$ yr for $q_o = 0$. Less than $\sim 25\%$ decrease in $t_{\rm cool}$ if $\beta = 1/2$ (rather than $\beta = 2/3$ assumed here).

8. THE NON-THERMAL COMPONENT

Support for the non-thermal nature of most of the unresolved X-ray emission is shown in Figure 2 where the X-ray spectral luminosity of this component (from our spectral analysis) is plotted against the spectral luminosity of the radio core (see Table 6). Although NGC 326 is shown, its X-ray spectral luminosity is highly uncertain and is likely to be overestimated (see caption). The other sources shown are consistent with proportionality between the X-ray and radio emission, in support of a model where the X-rays originate as non-thermal emission from the inner regions of a parsec-scale radio jet.

The X-ray (power-law) spectral indices (Table 3) are not well constrained, but are generally consistent with values for BL Lac objects (Worrall & Wilkes 1990), the sources proposed as low-power radio galaxies with relativistic radio jets in the line of sight of the observer (e.g., Wardle, Moore & Angel 1984). Our results are in qualitative agreement with such a 'unified' model.

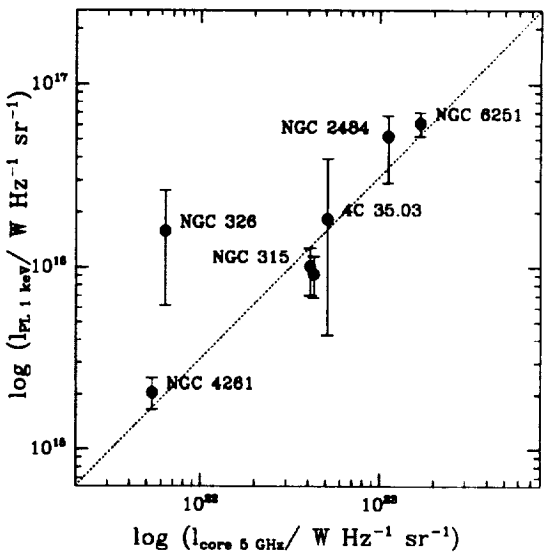

Figure 2. 1 keV X-ray spectral luminosity for the power-law component in the two-component spectral fit plotted against 5 GHz radio-core spectral luminosity (see Table 6). The X-ray errors are 1σ for one interesting parameter, allowing the other parameters to vary. An additional large systematic error should be applied to the derived X-ray value for NGC 326 since the source is dominated by non-radially symmetric extended emission (see §2) and the unresolved component may contain substantial thermal emission (see §5). The dotted line is of slope unity.

Table 6: Non-thermal Emission

Object	$S_{\rm PL}$ (1 keV) nJy	$S_{\rm core}$ (5 GHz) mJy	$S_{\rm Tot}$[b] (5 GHz) mJy	Radio Refs.
NGC 4261	112(+23, −22)	293	4200	1,6,7
NGC 315[a]	107(+28, −33)	450	1050	2,6,7
...	97(+24, −25)	...	...	...
4C 35.03	39(+44, −30)	106	1000	3,6,7
NGC 6251	308(+44, −47)	850	1550	4
NGC 2484	84(+25, −37)	190	1050	3,6,7
NGC 326	18(+12, −11)	8.6	600	5,6,7

a. First and second exposures (Table 1) listed separately.
b. $\sim 15\%$ uncertainty
Refs.– 1: Birkinshaw & Davies 1993 – 2: Venturi et al. 1993 – 3: Giovannini, Feretti & Comoretto 1990 – 4: Jones et al. 1986 – 5: Fomalont 1993 (private communication) – 6: Becker, White & Edwards 1991 – 7: Gregory & Condon 1991.

9. CONCLUSIONS

The ROSAT spectral and spatial results are self-consistent in indicating that low-power radio galaxies emit at least two components of X-rays. One component is resolved. It can be modeled spatially with a β model, and a thermal origin is also supported by spectral fitting. The hot gas is of a dimension ranging from galaxy size (for NGC 4261 and NGC 315) to cluster size (for NGC 326). Only the gas of galaxy scale cools fast enough that a cooling flow may have begun.

The second X-ray component is unresolved. It is likely to be predominantly thermal in NGC 326, which differs from the other sources in that the resolved emission is relatively stronger, larger, and non-radially symmetric. For the other sources, a proportionality between the unresolved X-ray and core radio emission supports the dominant origin for the unresolved X-ray emission as non-thermal radiation from the inner regions of a parsec-scale radio jet. A non-thermal origin for most of the unresolved emission in NGC 6251 has already been argued on the basis of more detailed work by Birkinshaw & Worrall (1993).

The sources studied show an order of magnitude range in the relative strength of the unresolved and resolved emission, and, since we are measuring components only on angular sizes between 15″ and 5′, the linear sizes of emission which can be resolved is influenced by the galaxy redshifts. In the closest radio galaxies, NGC 4261 and NGC 315, low-level thermal emission of group or cluster dimension becomes hard to measure because of its relatively large angular size. Evidence for such emission around NGC 4261 has been found by Davis et al. (1993), perhaps explaining the small apparent excess over our model profile at radii $2' - 4'$ (fig. 1a). Conversely, gas of galaxy dimension in the other sources would lie within the PRF of the PSPC; however, an argument limiting this to a small fraction of the core X-radiation in NGC 6251 has been presented by Birkinshaw & Worrall (1993) based on detailed X-ray spectral analysis.

ROSAT has provided a major advance in radio-galaxy X-ray research by showing that a mixture of resolved (thermal) and unresolved emission is typical. This situation appears to apply also to high-power radio galaxies; Worrall et al. (1993) report similar findings in the $z = 1$, high-power, radio galaxy 3C 280.

The measurement of multiple X-ray emission components has implications for models in which BL Lac objects are low-power radio galaxies with their parsec-scale relativistic jets in the line of sight. Padovani & Urry (1990) used *Einstein* Observatory data to construct X-ray luminosity functions for BL Lac objects and radio galaxies assuming that the intrinsic luminosity of the jet is some fixed fraction of an unbeamed luminosity. Birkinshaw & Worrall (1993) argued on the basis of results for NGC 6251 that thermal X-ray emission may be the source of the required unbeamed X-ray emission. However, the current work would not appear to support this suggestion. Table 3 shows that in every case the power-law luminosity (assuming that the X-rays are radiated isotropically) exceeds the thermal luminosity. Thus, by Padovani and Urry's definition every object would be classed as a BL Lac object rather than a radio galaxy, in violation of the selection of objects used to construct the luminosity functions. Consistency would appear to require part of the measured unresolved X-ray emission to be unbeamed, perhaps through a contribution from unresolved hot gas or because of a velocity or collimation gradient in an X-ray-emitting jet (Ghisellini & Maraschi 1989; Maraschi, Celotti & Ghisellini 1992). Further discussion and more detailed results for individual sources will be presented elsewhere.

We thank Walter Jaffe and Brian McNamara for transmitting pre-publication results on the neutral gas in NGC 4261, and Martin Elvis and the referee for comments which improved the paper. Our work was funded by NASA grants NAG5-1882 and NAG5-2312, and NASA contract NAS8-39073.

REFERENCES

Becker, R.L., White, R.L. & Edwards, A.L. 1991, ApJS, 75, 1
Birkinshaw, M. & Davies, R.D. 1993, in preparation
Birkinshaw, M. & Worrall, D.M. 1993, ApJ, 412, 568
Biretta, J.A., Stern, C.P. & Harris, D.E. 1991, AJ, 101, 1632
Cavaliere, A. & Fusco-Femiano, R. 1978, A&A, 70, 677
Davis, D.S. et al. 1993, in preparation
deVaucouleurs, G., deVaucouleurs, A., Corwin, H.G., Buta, R.J., Paturel, G. & Fouqué, P. 1991, Third Reference Catalogue of Bright Galaxies (Berlin: Springer-Verlag)
Elvis, M. & Lawrence, A. 1988. ApJ, 333, 161
Fabbiano, G., Gioia, I.M. & Trinchieri, G. 1989, ApJ, 347, 127
Fabbiano, G., Miller, L., Trinchieri, G., Longair, M. & Elvis, M. 1984, ApJ, 277, 115
Fabricant, D. & Gorenstein, P. 1983, ApJ, 267, 535
Feigelson, E.D., Schreier, E.J., Delvaille, J.P., Giacconi, R., Grindlay, J.E., Lightman, A.P. 1981, ApJ, 251, 31
Feigelson, E.D. & Berg, C.J. 1983, ApJ, 269, 400
Feretti, L., Spazzoli, O., Gioia, I.M., Giovannini, G. & Gregorini, L. 1990. A&A, 233, 325
Forman, W., Jones, C. & Tucker, W. 1985, ApJ, 293, 102
Ghisellini, G. & Maraschi, L. 1989, ApJ, 340, 181
Giovannini, G., Feretti, L. & Comoretto, G. 1990, ApJ, 358, 159
Gregory, P.C. & Condon, J.J. 1991, ApJS, 75, 1011
Hasinger, G., Turner, T.J., George, I.M. & Boese, G. 1992, NASA/GSFC/OGIP, Calibration Memo CAL/ROS/92-001
Jaffe, W. & McNamara B.R. 1993, in preparation
Jones, D.L. et al. 1986, ApJ, 305, 684
Maraschi, L., Celotti, A. & Ghisellini, G. 1992, in Physics of Active Nuclei, eds. W.J.Duschl & S.J.Wagner (Berlin: Springer-Verlag), 605
Max Planck Institut für Extraterrestrische Physik (MPE) 1992, ROSAT Newsletter number 10
Morganti, R., Fanti, R., Gioia, I.M., Harris, D.E., Parma, P. & de Ruiter, H. 1988, A&A, 189, 11
Padovani, P. & Urry, C.M. 1990, ApJ, 356, 75
Pfeffermann, E. *et al.*, 1987, in Soft X-ray Optics & Technology, eds. E.-E. Koch & G. Schmahl, Proc. SPIE, 733, 519
Raymond, J.C. & Smith, B.W. 1977, ApJS, 35, 419
Sarazin, C.L. 1986. Rev.Mod.Phys., 58, 1
Schreier, E.J., Feigelson, E., Delvaille, J., Giacconi, R., Grindlay, J., Schwartz, D.A. & Fabian, A.C. 1979, ApJ, 234, L39
Schreier, E.J., Gorenstein, P. & Feigelson, E.D. 1982, ApJ, 261, 42
Stark, A.A., Gammie, C.F., Wilson, R.W., Bally, J., Linke, R.A., Heiles, C. & Hurwitz, M. 1992, ApJS, 79, 77
Trümper, J. 1983, Adv.Space.Res., 2, 241
Ulrich, M.-H. 1989, in BL Lac Objects, eds. L. Maraschi, T. Maccacaro & M.-H. Ulrich (Berlin: Springer-Verlag), 45
Venturi, T., Feretti, L., Giovannini, G., Comoretto, G. & Wehrle, A.E. 1993, ApJ, 408, 81
Wardle, J.F.C., Moore, R.L. & Angel, J.R.P. 1984, ApJ, 279, 93
Worrall, D.M. & Wilkes B.J. 1990, ApJ, 360, 396
Worrall, D.M. et al. 1992, in Data Analysis in Astronomy IV, eds. V. Di Gesu et al. (New York: Plenum Press), 145
Worrall, D.M., Lawrence, C.R., Pearson, T.J. & Readhead, A.C.S. 1993, ApJ (Letters), in press

Procs. IAU Symp. 159, "AGN Across the Electromagnetic Spectrum", Kluwer, in press (1993)

NEW X-RAY RESULTS ON RADIO GALAXIES

D.M. WORRALL and M. BIRKINSHAW
Harvard-Smithsonian Center for Astrophysics, Cambridge, MA 02138, U.S.A.

Abstract.
Prior to ROSAT, separation of X-ray components in radio galaxies has been limited to a few well-known sources, e.g., M 87 and Cen A. Now, from ROSAT PSPC measurements of the first six objects in our study of low-power radio galaxies, we find that both resolved (thermal) and unresolved X-ray emission in a single source is typical (Worrall & Birkinshaw 1993; ApJ, submitted). The angular size of, and fraction of luminosity in, the resolved X-ray emission varies between objects. There is evidence to relate the unresolved X-ray emission with the inner radio jet.

Our joint X-ray spatial fits to unresolved and resolved emission (characterized by a thermal β model) in the six radio galaxies are better than those to either component alone. Spectral fits to two components (a two-temperature gas, or a one-temperature gas plus a power law) are better than those to one component. One source, NGC 326, is anomalous: its X-ray-emitting gas is very extended (of cluster dimension) and asymmetric; more complex models are required here. Two X-ray components characterize each of the other sources adequately, as shown by the self-consistency of our spatial and spectral fits (Table 1).

The X-ray data alone do not determine whether the unresolved component is thermal or non-thermal, although for NGC 6251, where the unresolved component is dominant, we have used gas-confinement properties to argue for a non-thermal origin (Birkinshaw & Worrall 1993; ApJ, 412, 568). A proportionality between the X-ray power-law (from our two-component fit) and radio-core luminosity densities (Fig. 1) further supports an origin for most of the unresolved X-ray emission as non-thermal radiation from the inner regions of a parsec-scale radio jet.

Table 1
% counts in unresolved/total (spatial fit) & power law/total (spectral fit)

Galaxy	Spatial Fit[a]	Spectral Fit[a]
NGC 4261	51 ± 4	52 ± 6
NGC 315[b]	61 ± 7	57 ± 9
...	41 ± 5	54 ± 7
4C 35.03	29 ± 6	52 ± 15
NGC 6251	93 ± 5	78 ± 6
NGC 2484	65 ± 9	76 ± 15
NGC 326	10 ± 2	25 ± 2

a. 1σ statistical errors for best-fit model; systematic errors in model parameters not included.

b. Two PSPC exposures listed separately.

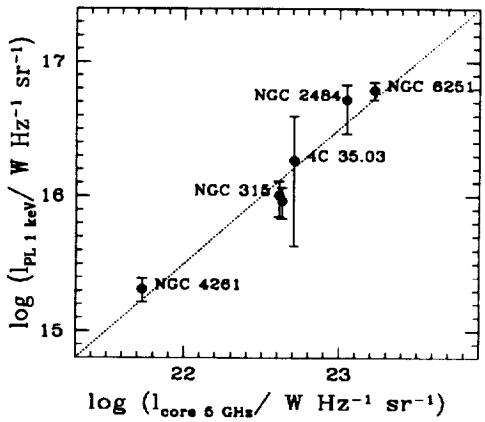

Fig. 1. X-ray power-law and radio core luminosity densities; correlation supports association of the unresolved X-ray component with the inner radio jet. (NGC 326 excluded; see text.)

Procs. ADASS '93, "Astronomical Data Analysis Software and Systems III", ASP Conference Series, in press (1993)

Analysis Techniques for a Multiwavelength Study of Radio Galaxies

D.M. Worrall and M. Birkinshaw

Harvard-Smithsonian Center for Astrophysics, Cambridge, MA 02138

Abstract.

Our multiwavelength study of radio galaxies requires the use of a mixture of home-grown software and widely-used analysis packages. We outline current procedures and provide an assessment directed at software developers.

1. Introduction

Our study of radio galaxies combines X-ray, radio, and optical data to address scientific objectives including: (a) Are the radio jets in pressure balance with an external hot medium? (b) What is the rate of fuel supply to the active nuclei? (c) What physical mechanisms produce the nuclear and jet emission?

Our current data-reduction, display, and analysis requires the use of IRAF, AIPS, SM, MONGO, and home-grown FORTRAN programs, and simplifications are made in the analysis due to the current limitations of the tools and procedures. Work on the radio galaxy NGC 6251 is used to illustrate our current methods, in the interest of stimulating discussion of improved analysis tools and procedures. Scientific results can be found in Birkinshaw & Worrall (1993) and Worrall & Birkinshaw (1994). Details concerning the software packages can be found elsewhere in this book and in volumes I and II of the series.

2. Comparison of X-ray, Radio, and Optical Images

We performed the basic reduction of our VLA radio data and ROSAT PSPC X-ray data for NGC 6251 using the AIPS and IRAF/PROS systems, respectively. We then transferred the X-ray image to AIPS (via FITS-format conversions) and used the 'regrd' and 'hgeom' tasks to re-grid the radio image to match the header of the X-ray image; this included precession between epochs B1950 and J2000. The re-gridded radio image was transferred to IRAF and an overlay contour plot (produced by the IRAF/PROS/imcontour task) of the radio image was drawn on the X-ray image using IRAF. An SAOimage display of the result was converted into a PostScript file using a Unix X-windows to PostScript conversion procedure ('xwd' followed by 'xwd2ps'); the resulting plot is shown as Figure 1a.

The X-rays are only slightly resolved (see §3) and radially symmetric. No X-ray emission is detected associated with the 4-arcmin radio jet. IRAF/PROS tasks and home-grown IRAF scripts were run to quantify these statements.

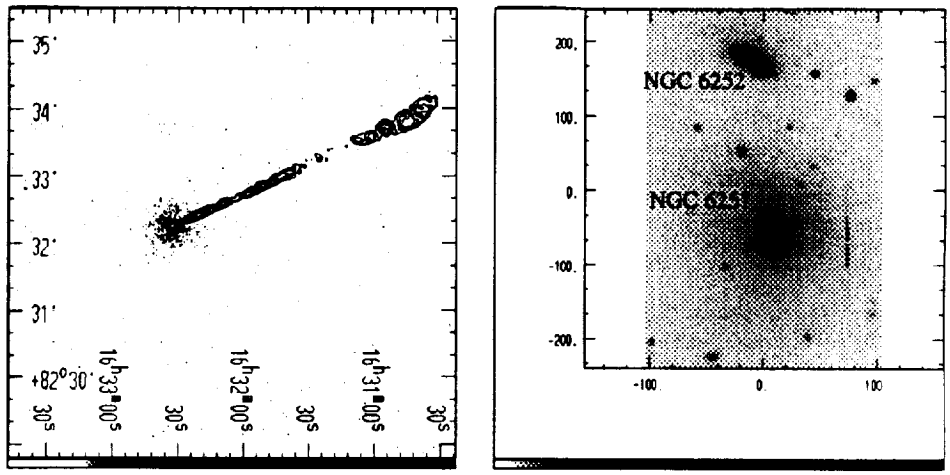

Figure 1. (a) Contour plot of 330 MHz VLA A-array reduced data overlayed on ROSAT PSPC X-ray image. The X-rays are concentrated at NGC 6251's core. (b) KPNO CCD red image of similar, but not identical, spatial scale (0.59 arcsec/pixel).

Our KPNO CCD red image was analyzed using IRAF (Fig. 1b). By chance, the scale is similar to that of Figure 1a, and north points up on both figures; celestial-coordinate-system parameters need adding to the optical image before overlays are possible. Display and plotting used the same method as for Figure 1a. X-rays are not detected from the companion galaxy NGC 6252.

3. X-ray Extent and Multiwavelength Emission from the Radio Jet

The energy distribution and radial profile of the X-ray photons (Fig. 1a) were extracted using IRAF/PROS. Home-grown FORTRAN software was used to fit the radial profile to source models convolved with the energy-dependent radially-symmetric ROSAT PSPC point response function (PRF; Fig. 2a), using the technique described by Birkinshaw (1994). The best fit is to a point-source (narrow curve) plus hot gas described by a hydrostatic β-model (broad curve). The plot was made using the FORTRAN interface to the SM package which in turn allows PostScript output easily.

The most prominent feature in the radio jet was modeled as synchrotron emission, and model parameters were found by comparing the calculated multi-wavelength spectrum with observations (including the X-ray upper limit). The model fitting was achieved using home-grown FORTRAN software and the MONGO plotting package (Fig. 2b); a similar fit for M 87 is shown for comparison.

4. Line of Sight Absorption and Galaxy Environment

An independent measure of the amount of X-ray absorbing gas along the line of sight helps us to constrain our X-ray spectral-model fits. We mapped NGC 6251

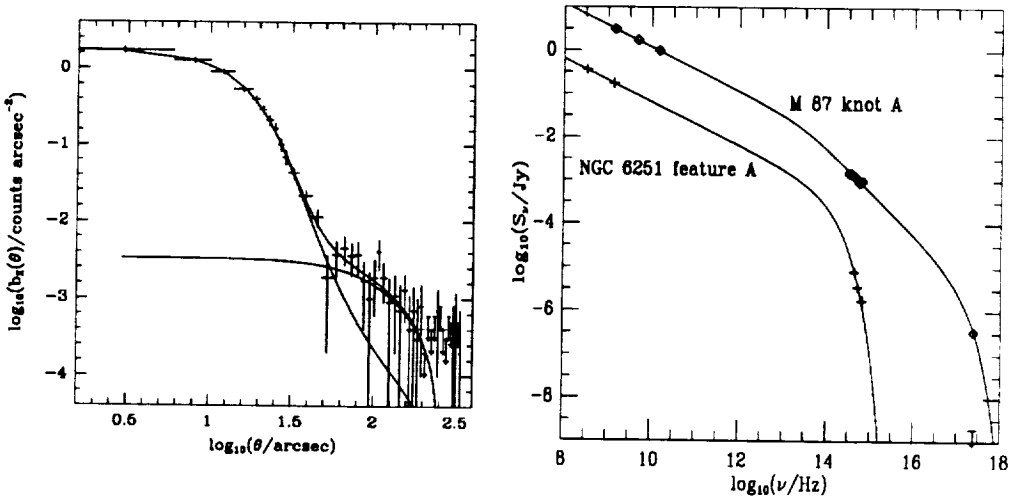

Figure 2. (a) X-ray radial profile and best-fit PRF-convolved two-component model. (b) Comparison of multiwavelength synchrotron spectrum with observations for the most prominent feature in NGC 6251's jet and for knot A of another radio galaxy, M 87.

with the VLA over a range of frequencies sensitive to HI absorption at velocities associated with the radio galaxy and intervening material. The spectral channel maps were analyzed using AIPS. It was then necessary for several hundred numbers to be typed in by hand and averaged for overlapping bins to produce an HI spectrum (Fig. 3a). The absence of strong features in this spectrum limits the amount of X-ray absorption and helps us to constrain our X-ray spectral-model fits (not shown) which are accomplished using IRAF/PROS.

A catalog was searched for bright galaxies in the vicinity of NGC 6251. These galaxies were plotted and labeled with velocities using SM (Fig. 3b); this is a reference plot for us, not intended to be of publication quality. We have MMT spectra (not shown) which we are analyzing with IRAF to measure velocities for several galaxies in the field. The dispersion of these velocities constrains the temperature of hot gas which can be associated with any galaxy groups, and further helps us to determine the correct X-ray spectral model.

5. Assessment

- Major packages are good at providing standard data reduction and calibration routines. Transfer of images between these packages (e.g., IRAF and AIPS) is easy and convenient via the FITS format.

- All ground-based telescope systems need to make their best attempts at attaching the celestial coordinate system to their images, as is already true for radio interferometer and space-based systems. Re-gridding, mosaicing, and correcting distortions are difficult problems affecting our ability to overlay images; more convenient software would help.

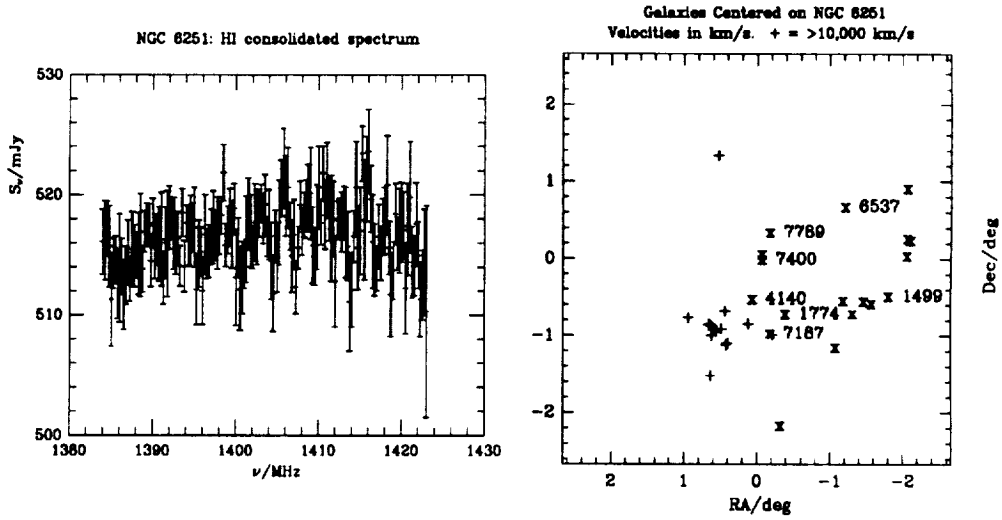

Figure 3. (a) No strong HI absorption features are seen in the radio spectrum. (b) Positions and velocities (where available) of bright nearby galaxies extracted from a catalog.

- The electronic preparation of papers and posters requires analysis packages to produce publication-quality output graphics in encapsulated PostScript. Switches should be provided for turning on and off information text within or surrounding the plot (as in e.g., the 'imcontour' task in IRAF/PROS).
- Our scientific objectives require home-grown specialized science programs which use results from the major packages.
  - Since coding inside major packages requires substantial experience, it is more convenient for us to write specialized code as external home-grown routines; more provision of dummy tasks with places for user-supplied analysis code (e.g., 'taffy' in AIPS) would encourage us to develop code within major packages.
  - Transfer of *results* (cf images) is inconvenient; we would like major packages to provide results in ASCII files of user-definable format for transfer to our specialized science code.

Acknowledgments. Support from NASA grant NAG5-1882 and contract NAS8-39073 is gratefully acknowledged.

References

Birkinshaw, M. 1994, this volume

Birkinshaw, M. & Worrall, D.M. 1993, ApJ, 412, 568

Worrall, D.M. & Birkinshaw, M. 1994, ApJ, in press

SEPARATION OF X-RAY EMISSION COMPONENTS IN RADIO GALAXIES

D.M. Worrall and M. Birkinshaw
Harvard-Smithsonian Center for Astrophysics, Cambridge, MA 02138-1596

Email ID
dmw@cfa.harvard.edu, mbl@cfa.harvard.edu

ABSTRACT

One of ROSAT's major achievements has been its ability to separate X-ray emission components in many radio galaxies, where this was previously possible only for a very few well-known sources, e.g., M 87 and Cen A. The dominant X-ray emission mechanism in radio galaxies as a class was unclear, with correlations between the X-ray and radio emissions used on one hand to argue for a nuclear origin for the X-rays, and on the other hand for a thermal origin. Now, with ROSAT we find the presence of both resolved (thermal) and unresolved emission to be typical.

Our results are illustrated with PSPC data from the first six radio galaxies in our study. Spectral and spatial measurements independently support the presence of multiple emission components. The resolved emission can be modeled as thermal radiation from gas of galaxy, group, or cluster dimension depending on object. The unresolved emission may be thermal or non-thermal. Evidence is presented to support a non-thermal origin for most of the unresolved emission: for NGC 6251, where this component is dominant, gas-confinement properties argue against a thermal origin; for the sample as a whole, a proportionality between the unresolved X-ray and the radio-core luminosity densities supports the existence of non-thermal X-ray radiation from the inner regions of a parsec-scale radio jet. Our results have implications for the unification of BL Lac objects with low-power radio galaxies; part of the unresolved X-ray emission in the radio galaxies is probably unbeamed.

1. X-ray Observations and Data Reduction

The radio galaxies listed in Table 1 are the first sources which were observed during two of our programs: to study a subsample of radio galaxies which Ulrich (1989) proposed are drawn from the parent population of BL Lac objects, and to study the emission in and around low-power radio galaxies with prominent radio jets.

For data reduction we used the Post Reduction Off-line Software (PROS; Worrall et al. 1992) and additional software which we developed to convolve the energy-dependent PSPC point response function (PRF; Hasinger et al. 1992) with radially-symmetric spatial models. Only counts within the energy band for which the PRF is well modeled (0.2 – 1.9 keV) are used. NGC 326 is the only source to show obvious *asymmetric* extended emission; the analysis presented here is for a pie-slice region where the source is least extended, and it is presented only to provide a qualitative comparison with the other sources.

For each radial profile, best fits were determined to models consisting of an unresolved component, a β model which is appropriate for gas in hydrostatic

To appear in the Proceedings of the November 1993 ROSAT Science Symposium, Maryland. AIP Conference Proceedings.

Table 1: PSPC Observations

Object	Name B1950	z	Date	Exposure[a](s)
NGC 315	0055+300	0.0165	1992 Jan 17–Feb 1	10,343
			1992 Jul 19–21	17,869
NGC 326	0055+265	0.047	1992 Jul 24–29	20,969
4C 35.03	0206+355	0.0375	1992 Jul 24–27	14,843
NGC 2484	0755+379	0.0413	1991 Oct 30–Nov 1	15,172
NGC 4261	1216+061	0.0073	1991 Dec 24–30	22,042
NGC 6251	1637+826	0.024	1991 Mar 13–16	14,830

a. Time used in analysis, excluding some intervals of high background.

equilibrium (e.g., Sarazin 1986), and a combination of an unresolved component and a β model. The combined fits (Fig. 1) give a significantly smaller value for χ^2 than a fit to either model alone in all cases except for NGC 315, for which the β-model component is barely resolved. To check that systematic errors in the aspect determination have a negligible effect on our results, we applied our analysis to two BL Lac objects and two quasars spanning similar exposure times and net counts to the radio galaxies; all fitted an unresolved component and excluded the presence of additional resolved X-ray emission of similar strength to that detected in the radio galaxies.

The same net counts which give the radial profiles of Figure 1 are used for our spectral fitting. The presence of a resolved X-ray component suggests at least some thermal emission, but for all sources the fits improve if either a power-law model or a second thermal model is added. In either case, the percentage of counts in the unresolved component agrees well with that in one of the spectral components, indicating self-consistency between our spectral and spatial analyses; in the case of a power-law plus thermal spectral model, we are required to identify the power law with the unresolved emission (as is physically most reasonable) to get agreement (Fig. 2). The spectral fits to a power-law plus thermal model give spectral energy indices of $\alpha \sim 0.8$, but with large errors, and the temperatures are tightly distributed about $kT \sim 0.7$ keV (except for the anomalous case of NGC 326). The power-law indices, although not well constrained, are generally consistent with values for BL Lac objects (Worrall & Wilkes 1990), the sources proposed as low-power radio galaxies with their relativistic jets pointed towards the observer. The fits to two thermal components give one with $kT < 1$ keV and the other with $kT > 1$ keV.

2. The Nature of the Unresolved X-ray Emission

The X-ray data alone do not determine the nature of the unresolved component, but the integrated emission of discrete X-ray sources similar to those in spiral galaxies is unimportant; the X-ray luminosities of all the separate spectral components for the radio galaxies lie at least an order of magnitude above the X-ray/optical correlation for spiral galaxies of Fabbiano, Gioia & Trinchieri (1989), and are comparable with or exceed 10^{34} W (the limiting X-ray luminosity of spiral galaxies). The resolved emission is therefore certainly hot gas; the measured scale-size associates it primarily with the galaxy for NGC 4261 (but see indication for a larger scale-size excess in Fig. 1, and the paper by Mushotzky

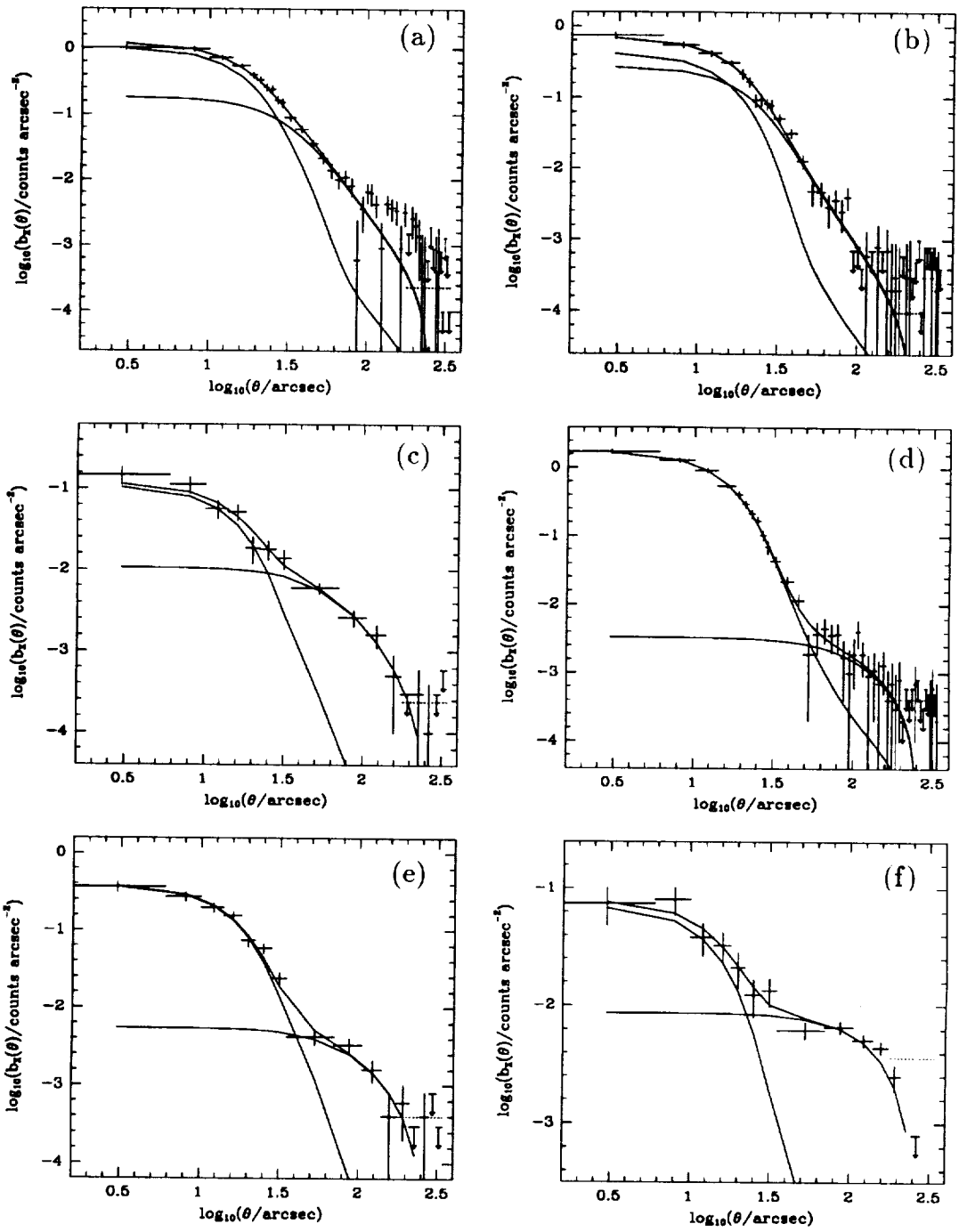

Figure 1: Background-subtracted X-ray radial profiles for the radio galaxies in order of increasing intrinsic core-radius of the β model. (a) NGC 4261, (b) NGC 315, second exposure, (c) 4C 35.03, (d) NGC 6251, (e) NGC 2484, and (f) NGC 326. Data are fit to a combination of an unresolved component (narrow curve) and a β model (broad curve) convolved with the PSPC PRF. The dotted curve shows the contribution, taken into account in the fitting, of the model to the background annulus. (Figure taken from Worrall & Birkinshaw 1994.)

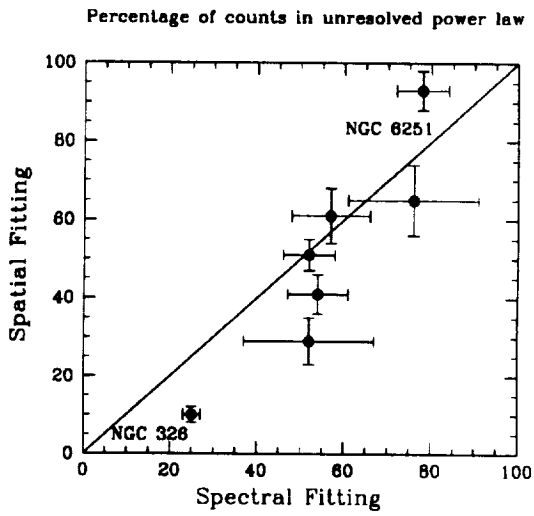

Figure 2: The fraction of counts in the unresolved component from spatial fitting agrees well with that in the power law from the spectral fitting, especially considering that these errors do not include uncertainties in the model parameters and the spatial analysis did not take into account the different spectral distributions of the β model and the unresolved component. The discrepancy for NGC 326 is not surprising given the inadequacies of a radially-symmetrical analysis for its complex emission region. The discrepancy for NGC 6251 is discussed in the text.

in this volume) and NGC 315, with cluster gas for NGC 326, and with group gas for the other sources.

The unresolved X-ray component is allowed either a thermal or non-thermal origin from our X-ray analysis alone. However, for NGC 6251, which has the brightest unresolved emission, a detailed analysis has shown that this inner emission requires a small ($\sim 20\%$) contribution of cool ($kT \sim 0.5$ keV) gas added to either a power-law or a hot ($kT \sim 5$ keV) thermal component (Birkinshaw & Worrall 1993; but see also Birkinshaw & Worrall, this volume). The difficulty in interpreting the dominant spectral contribution to the unresolved emission as thermal is the high temperature; neither the stars in NGC 6251 nor the surrounding galaxies display a sufficiently large velocity dispersion for ~ 5 keV gas to be hydrostatically confined. This points to the interpretation of the unresolved X-ray component of NGC 6251 being $\sim 80\%$ non-thermal and $\sim 20\%$ 0.5 keV gas (lowering its position slightly in Fig. 2).

General support for the non-thermal nature of most of the unresolved X-ray emission is shown in Figure 3 where the X-ray spectral luminosity of the fitted power-law component is plotted against the spectral luminosity of the radio core. Although NGC 326 is shown in the figure, its X-ray spectral luminosity is highly uncertain and is likely to be overestimated (see caption). The other sources shown are consistent with proportionality between their X-ray and radio emissions, supporting a model where these X-rays are non-thermal emission from the inner regions of a parsec-scale radio jet.

3. Implications for Unified Schemes

The measurement of multiple X-ray emission components has implications for Unified Schemes in which BL Lac objects are low-power radio galaxies with their parsec-scale relativistic jets pointed towards the observer. Padovani & Urry (1990) used *Einstein* Observatory data to construct X-ray luminosity functions for BL Lac objects and radio galaxies assuming that the intrinsic luminosity of the jet is some fixed fraction of an unbeamed luminosity. Birkinshaw & Worrall (1993) argued on the basis of results for NGC 6251 that thermal emission may be the source of the required unbeamed X-rays. In NGC 6251 the emission interpreted as non-thermal outshines the thermal emission by a factor of

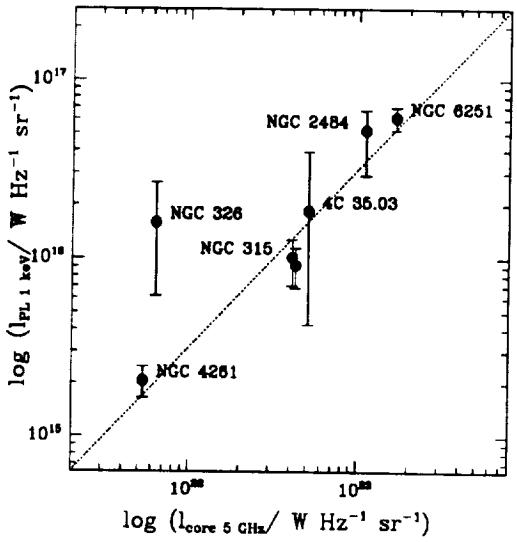

Figure 3: 1 keV X-ray spectral luminosity for the power-law component plotted against 5 GHz radio-core spectral luminosity. X-ray errors are 1σ for one interesting parameter, allowing the other parameters to vary. An additional large systematic error should be applied to the X-ray point for NGC 326; this source is dominated by non-radially symmetric extended emission and the unresolved component may contain substantial thermal emission. The dotted line is of slope unity. (Figure taken from Worrall & Birkinshaw 1994.)

~ 4, placing the source as 'transitional' between radio galaxies and BL Lac objects. The model parameters of Padovani & Urry predict that for $> 90\%$ of the radio-galaxy population the beamed emission should be $\lesssim 30\%$ of the unbeamed emission, and for $> 70\%$ of the population the beamed percentage drops to $\lesssim 1\%$. Since we find that all the sources under study here (with the exception of NGC 326) have a significant fraction of their emission unresolved on PSPC scales, consistency appears to require much of the unresolved X-ray emission to be unbeamed, perhaps through a contribution from hot gas or because of a velocity or collimation gradient in an X-ray-emitting jet (e.g., Ghisellini & Maraschi 1989; Maraschi, Celotti & Ghisellini 1992). We await approved observations of four of these galaxies with the ROSAT HRI to search for resolved components on spatial scales as small as $\sim 5''$ to test the fraction of the PSPC unresolved emission which might arise from thermal gas.

Further details of this work can be found in Worrall & Birkinshaw (1994). The work was funded by NASA grants NAG5-1882 and NAG5-2312, and NASA contract NAS8-39073.

References

Birkinshaw, M. & Worrall, D.M. 1993, ApJ, 412, 568
Fabbiano, G., Gioia, I.M. & Trinchieri, G. 1989, ApJ, 347, 127
Hasinger, G., Turner, T.J., George, I.M. & Boese, G. 1992, NASA/GSFC/OGIP. Calibration Memo CAL/ROS/92-001
Ghisellini, G. & Maraschi, L. 1989, ApJ, 340, 181
Maraschi, L., Celotti, A. & Ghisellini, G. 1992, in Physics of Active Nuclei, eds. W.J.Duschl & S.J.Wagner (Berlin: Springer-Verlag), 605
Padovani, P. & Urry, C.M. 1990, ApJ, 356, 75
Sarazin, C.L. 1986, Rev.Mod.Phys., 58, 1
Ulrich, M.-H. 1989, in BL Lac Objects, eds. L. Maraschi, T. Maccacaro & M.-H. Ulrich (Berlin: Springer-Verlag), 45
Worrall, D.M. & Wilkes B.J. 1990, ApJ, 360, 396
Worrall, D.M. & Birkinshaw, M. 1994, ApJ, in press
Worrall, D.M. et al. 1992, in Data Analysis in Astronomy IV, eds. V. Di Gesu et al. (New York: Plenum Press), 145

X-RAY EMISSION IN POWERFUL RADIO GALAXIES AND QUASARS

D.M. Worrall
Harvard-Smithsonian Center for Astrophysics, Cambridge, MA 02138-1596
and
C.R. Lawrence, T.J. Pearson, A.C.S. Readhead
OVRO 105-24, California Institute of Technology, Pasadena, CA 91125

Email ID
dmw@cfa.harvard.edu

ABSTRACT

ROSAT is the first mission to have detected X-ray emission in radio galaxies which are both powerful ($l_{178\ \mathrm{MHz}} > 10^{27}$ W Hz^{-1} sr^{-1}) and distant ($z > 0.4$), enabling tests of "unified schemes" through a comparison of the X-ray and radio properties of powerful quasars and radio galaxies. These radio galaxies are faint in X-rays, but, nevertheless, ROSAT is capable of resolving any associated X-ray-emitting gas of cluster dimension.

We present ROSAT PSPC observations of two such radio galaxies and suggest that there is a component of unresolved X-ray emission in powerful, high-redshift radio galaxies which may be related to the radio core; this will be tested by ROSAT observations of other powerful radio galaxies.

1. ROSAT PSPC Observations of two Radio Galaxies

We observed 3C 220.3 and 3C 280 with the ROSAT PSPC during the AO1 pointed phase of the mission (Table 1). 3C 220.3 was undetected. 3C 280 gives 71 ± 12 net counts ($0.2 - 1.9$ keV). For absorption only by gas in our Galaxy, the PSPC spectrum fits a power law with $0.5 < \alpha < 2.0$ and a 1 keV flux density of 1.7 ± 0.9 nJy. Some intrinsic absorption and a steeper power-law slope cannot be excluded, although there are sufficient counts in the low-energy channels to suggest that such absorption has a column density $\lesssim 4 \times 10^{21}$ atoms cm^{-2}. A Raymond-Smith thermal spectral model also agrees with the data; for Galactic absorption only, any temperature $\gtrsim 0.4$ keV is acceptable.

Table 1

Radio Galaxy	z	log N_H [a]	ROR [b]	Date	Exposure Time (s)
3C 220.3	0.685	20.515	700072	1991 Feb 27	8,791
3C 280	0.998	20.086	700073	1991 Jun 2-3	48,051

a. Galactic values from Stark et al. (1992).
b. ROSAT Observation Request number

To appear in the Proceedings of the November 1993 ROSAT Science Symposium, Maryland. AIP Conference Proceedings.

2. X-ray Radial Profile of 3C 280

A point source alone gives a poor fit to the X-ray radial profile of 3C 280. A thermal β model (e.g., Sarazin 1986) gives a good fit, but the fit is improved still further if the source is modeled with a combination of a point source and β model (Fig. 1). The evidence for unresolved emission is suggestive, rather than compelling; moreover, the X-ray data do not distinguish between a thermal or a non-thermal origin for the possible unresolved component. However, the evidence for non-thermal X-rays from the nuclei of low-redshift radio galaxies (e.g., Fabbiano et al. 1984; Worrall & Birkinshaw 1994) and radio-loud quasars (e.g., Worrall et al. 1987) leads us to consider seriously the possibility that 3C 280 also emits non-thermal X-radiation from its radio core.

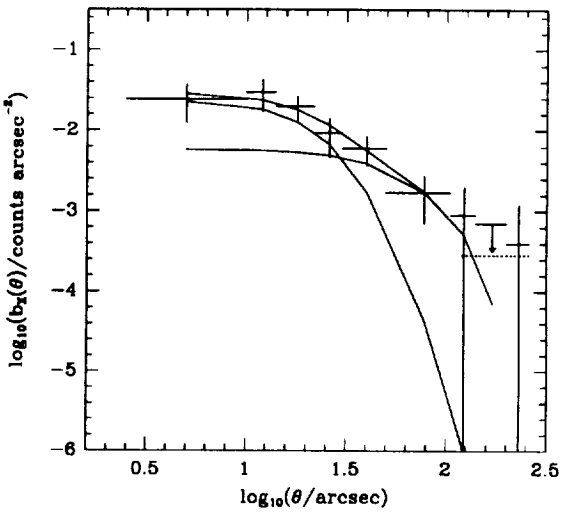

Figure 1: Background-subtracted PSPC radial profile for 3C 280. The best-fit model (upper curve), shown convolved with the PRF and background subtracted for comparison with the data, is a combination of an unresolved component (narrow curve) and a β model of core radius 65″ for $\beta = 2/3$ (broad curve). The dotted line shows the contribution of the model to the background annulus.

3. Radio Core-related X-rays in Quasars and Galaxies

In Figure 2 we compare the unresolved X-ray and core radio emissions for the two radio galaxies with those of radio-loud quasars which both have similar total (isotropic) power and were observed with the *Einstein* IPC (Wilkes et al. 1994). The luminosity-luminosity and flux-flux plots are similar because the sources lie in a relatively narrow band of redshift. The fraction, R, of 5 GHz flux density in the core component of the quasars has a bimodal distribution, in which core-dominated quasars with $R > 0.5$ (filled squares) can be clearly distinguished from lobe-dominated quasars (open squares). From Figure 2 we find:

(a.) A correlation between the core X-ray and radio emission in core-dominated quasars.

(b.) 3C 280 lies on an extrapolation of the correlation.

(c.) Lobe-dominated quasars have X-ray emission in excess of the correlation.

The inference from point (a), that the X-rays from core-dominated quasars are beamed, is supported by earlier work. Point (b) is most simply explained if the same core X-ray to radio relationship holds for radio galaxies as for core-

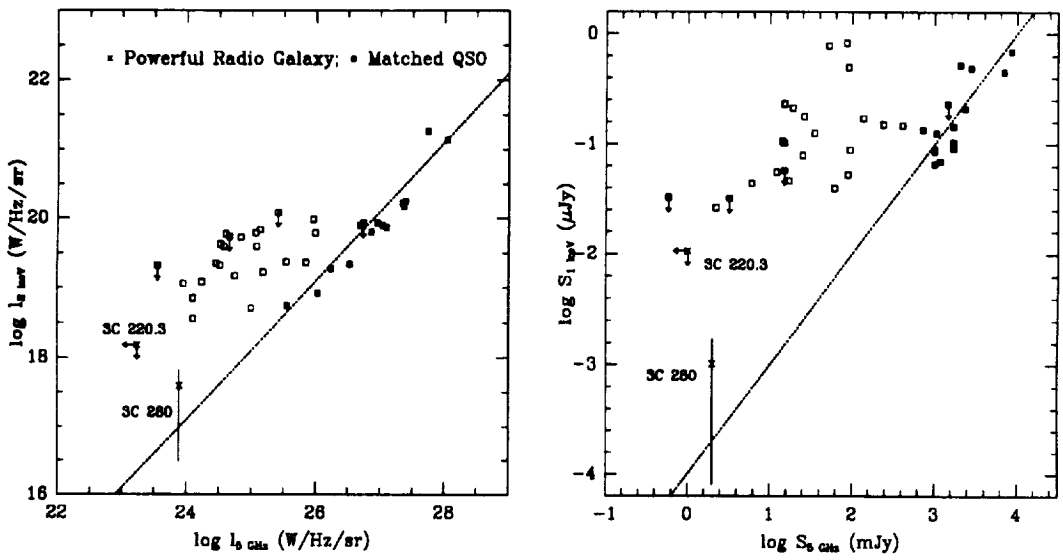

Figure 2: Core X-ray and radio flux densities for quasars (squares) matched in isotropic radio power with the radio galaxies 3C 220.3 and 3C 280. A line of slope unity (dotted) connects 3C 280 with the core-dominated quasars (filled squares), but not the lobe dominated quasars (open squares). Luminosity-luminosity (left) and flux-flux (right) plots are both presented to show that common-distance spreading has only a minor influence on the luminosity-luminosity plot and is not responsible for the correlation.

dominated quasars; this will be tested by ROSAT observations of other powerful radio galaxies. Point (c) suggests that lobe-dominated quasars contain an additional source of X-ray emission, possibly related to the nuclear X-ray emission in radio-quiet quasars. We infer that this compact X-ray component is obscured in radio galaxies, and dominated by beamed emission from the jet in core-dominated quasars. Further details of this work can be found in Worrall et al. (1994).

This work was primarily funded by NASA grants NAG5-1706 and NAG5-1882.

References

Fabbiano, G., Miller, L., Trinchieri, G., Longair, M. & Elvis, M. 1984, ApJ, 277, 115

Sarazin, C.L. 1986, Rev.Mod.Phys., 58, 1

Stark, A.A., Gammie, C.F., Wilson, R.W., Bally, J., Linke, R.A., Heiles, C. & Hurwitz, M. 1992, ApJS, 79, 77

Wilkes, B.J., Tananbaum, H., Worrall, D.M., Avni, Y., Oey, M.S. & Flanagan, J. 1993, ApJS, in press

Worrall, D.M. & Birkinshaw, M. 1994, ApJ, in press

Worrall, D.M., Giommi, P., Tananbaum, H. & Zamorani, G. 1987, ApJ, 313, 596

Worrall, D.M., Lawrence, C.R., Pearson, T.J. & Readhead, A.C.S. 1994, ApJ (Letters), in press

THE ASTROPHYSICAL JOURNAL, 420:L17–L20, 1994 January 1

EXTENDED AND COMPACT X-RAY EMISSION IN POWERFUL RADIO GALAXIES

D. M. WORRALL
Harvard-Smithsonian Center for Astrophysics, 60 Garden Street, Cambridge, MA 02138
AND
C. R. LAWRENCE, T. J. PEARSON, AND A. C. S. READHEAD
Owens Valley Radio Observatory, 105-24, California Institute of Technology, Pasadena, CA 91125
Received 1993 April 13; accepted 1993 October 13

ABSTRACT

We report *ROSAT* X-ray observations of two powerful radio galaxies. 3C 280 provides evidence for a mixture of unresolved and extended emission, with the latter produced by hot plasma of insufficient pressure to confine the radio lobes and insufficient density for a cooling flow to have begun. 3C 220.3 gives only an X-ray upper limit, but one consistent with our interpretation of the X-ray emission from powerful radio-loud AGNs in terms of obscured and unobscured components.

Subject headings: galaxies: active — galaxies: individual (3C 220.3, 3C 280) — radio continuum: galaxies — X-rays: galaxies

1. INTRODUCTION

A major question in the study of powerful radio sources is the extent to which they constitute a single population, with their range of observed properties primarily due to orientation effects caused by anisotropic emission and obscuration. Highly anisotropic emission at many frequencies is an inevitable consequence of the well-established presence of relativistic, self-absorbed, synchrotron plasma, and "unified" schemes explain the essential differences between core-dominated and lobe-dominated quasars by a combination of relativistic beaming and orientation. Such schemes also incorporate the unification of quasars with galaxies of comparable isotropic radio power (Readhead et al. 1978; Readhead 1980), in which anisotropic obscuration hides the broad emission-line regions (Antonucci 1982; Scheuer 1987; Barthel 1989). The current work explores the relationship between radio galaxies and quasars via comparisons of their X-ray and radio properties.

X-ray observations of *quasars* support relativistic beaming through measurement of flux densities which are lower than the predicted self-Compton emission of radio-emitting regions at rest (e.g., Marscher et al. 1979). Correlations of the X-ray emission with properties such as radio core strength, total isotropic radio power, optical emission, and mixtures thereof, have been claimed (Feigelson, Isobe, & Kembhavi 1984; Browne & Murphy 1987; Worrall et al. 1987).

X-ray data for *radio galaxies* of comparably high isotropic radio power to quasars are sparse. The powerful nearby galaxy Cygnus A is dominated by X-ray emission from the cluster in which the galaxy lies (Arnaud et al. 1984). Crawford & Fabian (1993) were the first to report an X-ray detection of a powerful radio galaxy at high redshift, 3C 356. The emission is extended and, by analogy with Cygnus A, they interpret it as due to cluster gas in a cooling flow. Separation of X-ray emission components has been difficult in the past even for nearby low-power radio galaxies (although *ROSAT* is now revealing that both unresolved and extended [thermal] components are typical [Worrall & Birkinshaw 1994]) and remains difficult for high-redshift galaxies.

Here we report *ROSAT* X-ray observations of the powerful high-redshift radio galaxies 3C 220.3 and 3C 280. 3C 280 is detected and provides evidence for a mixture of unresolved and extended X-ray emission. The ratio of X-ray to radio flux densities in the unresolved core component of 3C 280 is comparable to that in core-dominated *quasars* of similar redshift and extended radio power, suggesting that the unresolved X-ray component is synchrotron or self-Compton emission from a jet which is not highly obscured.

2. X-RAY DATA

We observed 3C 220.3 and 3C 280 in soft X-rays with the *ROSAT* Position-Sensitive Proportional Counter (PSPC; Trümper 1983; Pfeffermann et al. 1987) during the pointed phase of the mission (Table 1). SASS versions 5-3 (3C 220.3) and 5-4 (3C 280) were applied to the data to correct for instrumental effects and aspect. We performed additional analysis using the Post Reduction Off-line Software (PROS; Worrall et al. 1992). Conversion between observed count distribution and source flux uses the latest versions of the PSPC response matrix (No. 36) and effective area (No. 2-6). The PSPC point response function (PRF) has been modeled using analytical expressions for the on-axis scattering, focus, and intrinsic detector resolution contributions as a function of energy, applicable to the energy band 0.2–1.9 keV (spectral channels 6–29; Hasinger et al. 1992).

3C 220.3 was undetected; using a background annulus of radii 2′–5′ (excluding a nearby X-ray source), the 3 σ upper limit for the emission (0.17–2.4 keV) is 0.0037 counts s^{-1}. The conversion to flux density is spectrally dependent. If we assume the only absorption is in our Galaxy (Table 1), the 1 keV flux-density limit lies between ~ 5 and 12 nJy for a power-law spectral energy index α, ($S_\nu \propto \nu^{-\alpha}$), of 2.0–0.5. Later in this paper (see Fig. 3 below) we have adopted a 3 σ upper limit of 11 nJy, appropriate for $\alpha = 1.0$.

We filtered the 3C 280 PSPC data to remove times of high background which occurred on either side of some Earth occultations, leaving an exposure of 46,619 s. 3C 280 was detected with a significance of ~ 6 σ. Inside a circle of radius 35″, with background from an annulus of radii 3′–4′.3 (excluding two regions contaminated by other sources), 3C 280 gives 71 $\pm$ 12 net counts (0.2–1.9 keV). The X-ray power, which

TABLE 1

OBSERVATIONS

Object	z	log N_H[a]	ROR[b]	Date	Exposure Time (s)
3C 220.3.....	0.685	20.515	700072	1991 Feb 27	8791
3C 280	0.998	20.086	700073	1991 Jun 2–3	48051

[a] Galactic values from Stark et al. 1992.
[b] *ROSAT* Observation Request number.

is weakly dependent on spectral shape, is $\sim 1.0 \times 10^{36}$ W sr^{-1}. (Friedmann cosmology with $H_0 = 50$ km s^{-1} Mpc^{-1}, $q_0 = 0$, is used throughout.)

The spectrum of 3C 280 is poorly determined. For absorption comparable to that in the line of sight in our Galaxy, the spectrum agrees with a power law, with $0.5 < \alpha < 2.0$ and a 1 keV flux density of 1.7 ± 0.9 nJy. Intrinsic absorption and a steeper power-law slope cannot be excluded, although there are sufficient counts in the low-energy channels to suggest that such absorption is $\lesssim 4 \times 10^{21}$ atoms cm^{-2}. A Raymond & Smith (1977) thermal model also agrees with the data. For Galactic absorption, any temperature $\gtrsim 0.4$ keV is acceptable.

3. X-RAY SPATIAL EXTENT OF 3C 280

A maximum-likelihood centroid for the emission from 3C 280 was found using the PROS, and a background-subtracted radial profile with nine radial bins was extracted for energy range 0.2–1.9 keV (Fig. 1). The background region is described above, and the contribution of the source model in the background annulus (significant for extended models) was taken into account in our model fitting.

A point source alone gives a poor fit to the radial profile. The PRF, modeled assuming an energy weighting which reflects the apparent energies of the detected photons, gives a χ^2 of 60 when compared with the radial profile.

A β model (Cavaliere & Fusco-Femiano 1978; Sarazin 1986) with a core radius of 18″(+13″, −10″) and central brightness of 0.068 counts arcsec^{-2} gives a good fit. We have assumed $\beta = \frac{2}{3}$. The fit is formally rather too good ($\chi^2 = 2.5$ for 8 d.o.f.), suggesting that the uncertainties in the background have been overestimated, but the fit is improved still further if the source is modeled with a combination of a point source and β model. The amount of improvement is such that the F-test gives a 5% probability of such a large decrease in χ^2 by chance. The core radius is now 65″(+165″, −45″), the central brightness is 0.0074 counts arcsec^{-2}, and the unresolved component contains 60% of the net counts in the region for which the flux density was determined. The improvement of the fit with two components is insensitive to details of the binning.

A contour map of the X-ray emission from 3C 280 (Fig. 2) shows a possible slight asymmetry. The peak of the map is 6″ to the east of the maximum-likelihood centroid: a radial profile extracted with this new center is less smooth but gives qualitatively the same results as Figure 1. The radio lobes of 3C 280 extend only ~18″, roughly along an EW line (McCarthy, van Breugel, & Kapahi 1991; Liu, Pooley, & Riley 1992) and lie well within the X-ray extent. It is interesting that Gunn et al. (1981) have imaged optically two sources of comparable brightness separated by ~6″ and which lie roughly along a NE-SW line. The NE object has many narrow and slightly broadened emission lines (Lawrence et al. 1994) and provides the redshift for 3C 280. The SW object has not yet been observed spectroscopically, and it would be of great interest to determine if this is at the same redshift, since this would support a cluster hypothesis, and hence the existence of cluster gas, perhaps explaining the slight asymmetry in the X-ray emission.

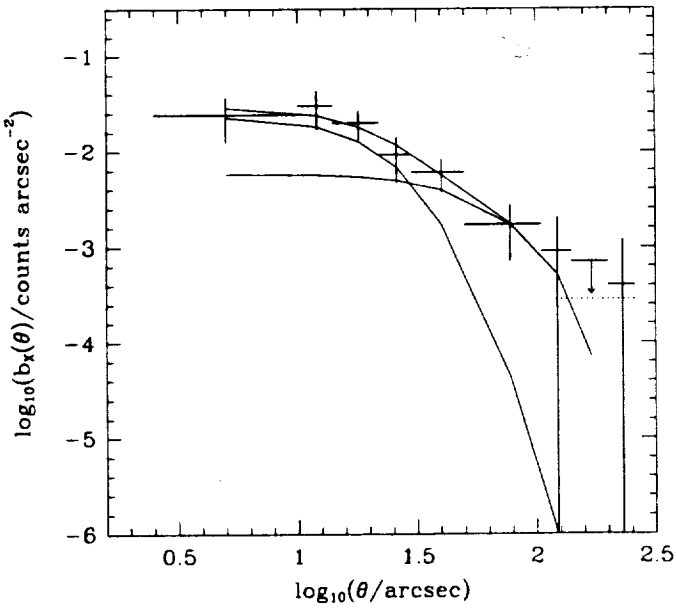

FIG. 1.—Background-subtracted radial profile for 3C 280. The best-fit model (*upper curve*), shown convolved with the PRF and background subtracted for comparison with the data, is a combination of unresolved component (*narrow curve*) and a β model of core radius 65″ (*broad curve*). The *dotted line* shows the contribution of the model to the background annulus.

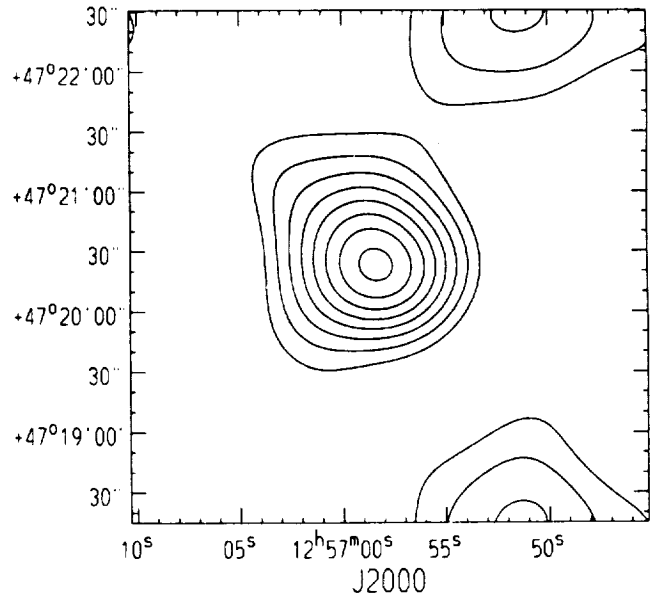

FIG. 2.—X-ray contour plot of 3C 280. The image has been smoothed with a Gaussian of $\sigma = 25$″, a beam size matching the circle of greatest detection significance. Contours are of significance 2–5.5 σ inclusive, in intervals of 0.5 σ. The edges of sources which have been excluded from the background region show up to the NW and SW. The axes show J2000 equatorial coordinates; an error in absolute position of up to ~10″ is possible due to a problem in *ROSAT*'s aspect determination (Max Planck Institut für Extratterrestriche Physik 1992).

4. DISCUSSION

We have found evidence for both unresolved and extended (and hence presumably thermal) X-ray emission in 3C 280. The evidence for unresolved emission is suggestive, rather than compelling; moreover, the X-ray data do not distinguish between a thermal or a nonthermal origin for the possible unresolved component. However, the evidence for nonthermal X-rays from the nuclei of low-redshift radio galaxies (Fabbiano et al. 1984; Readhead et al. 1983; Worrall & Birkinshaw 1994) and from quasars (e.g., Worrall et al. 1987) leads us to consider seriously the possibility that 3C 280 also emits nonthermal X-radiation from its nucleus. The alternative possibility, that all the X-rays are thermal, has been considered by Crawford & Fabian (1993) for 3C 356. We proceed on the assumption that the unresolved component in 3C 280 is real and from the nucleus.

Figure 3 compares the X-ray and radio-core flux densities of 3C 220.3 and 3C 280 with those of a carefully selected sample of quasars chosen to have low-frequency (isotropic) radio luminosities within a factor of ~ 20 of the radio galaxies. The quasar sample comprises all the quasars in the complete Pearson-Readhead, Hough-Readhead, and Caltech-Jodrell samples (Pearson & Readhead 1988; Hough & Readhead 1989; Wilkinson et al. 1993) with $z > 0.3$, and which were targets of the *Einstein Observatory* IPC (but not necessarily detected; Wilkes et al. 1994). The fraction, R, of 5 GHz flux density in the core component has a bimodal distribution, in which core-dominated quasars with $R > 0.5$ can be clearly distinguished from lobe-dominated quasars. For 3C 280 we plot the X-ray emission in the unresolved component only, found by multiplying the flux density from our spectral fitting (§ 2) with the percentage of counts in the unresolved component from our spatial fitting (errors are combined in quadrature). Although we have only upper limits for the flux densities of the components of interest for 3C 220.3, they are consistent with the interpretation of the emission of 3C 280 given below.

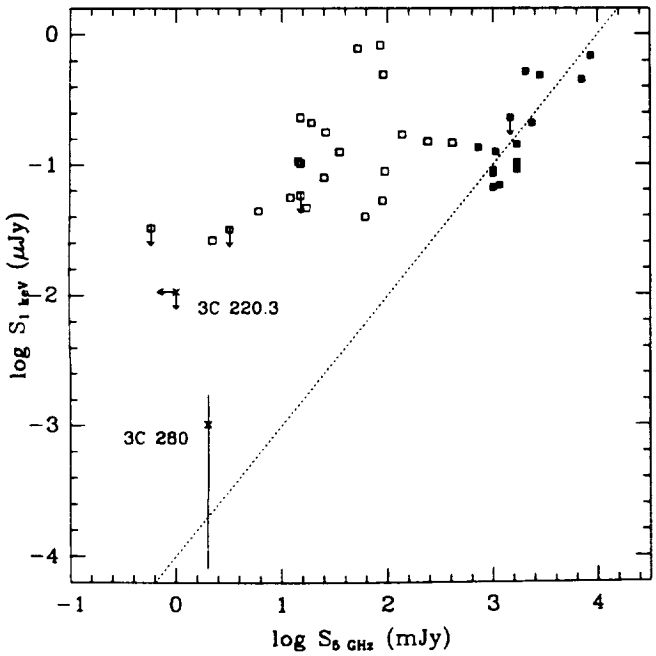

FIG. 3.—Core X-ray and radio flux densities for quasars (*squares*) matched in isotropic radio power with the radio galaxies 3C 220.3 and 3C 280. A line of slope unity (*dotted*) connects 3C 280 with the core-dominated quasars (*filled squares*), but not the lobe-dominated quasars (*open squares*).

In Figure 3 it is clear that for 3C 280 both the compact radio and the unresolved X-ray emission are about three orders of magnitude weaker than in core-dominated quasars of comparable isotropic radio luminosity. (All the sources lie in a relatively narrow band of redshift such that a plot in luminosity density looks similar.) The rough proportionality of X-ray and radio core flux densities between 3C 280 and the core-dominated quasars suggests that these emission components are related, as would be expected were the X-rays due to unobscured synchrotron emission or inverse Compton scattering in the radio emission regions. The radio and X-ray flux densities of the core-dominated quasars themselves are highly correlated (the Spearman rank correlation coefficient is 0.732, with a probability by chance of 0.0019), and seem to follow the same rough proportionality, adding support to this conclusion. For low-redshift ($z < 0.3$) radio galaxies, X-ray/core-radio correlations have been used previously to argue the importance of nuclear X-ray emission (Fabbiano et al. 1984), and in at least two galaxies, NGC 1275 and NGC 6251, evidence for such X-ray emission being of inverse Compton origin has been presented (Readhead et al. 1983; Birkinshaw & Worrall 1993). Here, by analogy, we suggest that the unresolved X-ray emission of a *powerful, high-redshift* radio galaxy may be related to its radio core.

The departure of the lobe-dominated quasars from X-ray/radio proportionality (Fig. 3) is evidence for an additional X-ray emission component. Core-dominated sources are believed to have bright cores because their jet emission, enhanced by relativistic boosting toward the observer, swamps all other emission components. However, the X-ray emission from radio-quiet quasars (usually interpreted as unboosted compact emission from the vicinity of the inner part of an accretion disk) is $\sim 50\%$ as luminous as in lobe-dominated quasars (e.g., Worrall et al. 1987). This implies that a significant fraction of the X-ray emission in lobe-dominated quasars may be compact and unboosted rather than jet-related. Figure 3 indicates that the compact emission is obscured (or perhaps absent) in powerful radio galaxies. A fuller discussion of this point will appear elsewhere.

The extended X-ray emission of 3C 280 has been modeled as a thermal gas. Table 2 uses the X-ray parameters of § 3 and equations (10), (11), (13), and (25) of Birkinshaw & Worrall (1993) to derive the central density, the pressure at 10″ from the core (assuming the source is in the plane of the sky), and the cooling time for gas within a core radius of the center. Only if all the X-rays are from gas of low temperature ($\lesssim 1$ keV, whereas $kT \sim 2$–5 keV is expected from the X-ray luminosity and temperature correlation for clusters; David et al. 1993) can a cooling flow have begun, and in the preferred two-component fit to the X-rays, the gas cooling time is greater than the Hubble time for all likely gas temperatures. However, only part of the unresolved X-ray emission need be thermal gas for a cooling flow in the inner regions to be accommodated.

Liu et al. (1992) have calculated the minimum-energy magnetic fields in the radio lobes of 3C 280 to be 4.5 and 6 nT, assuming a filling factor of unity and cylindrical symmetry. Using equation (1) of Miley (1980), this implies a minimum energy density, u_{min}, in the stronger lobe $\sim 3 \times 10^{-11}$ J m^{-3}. The corresponding minimum internal pressure of relativistic material, $\frac{1}{3}u_{min}$, is $\sim 1 \times 10^{-11}$ N m^{-2}, higher than the pressure provided by the ambient gas unless all the X-ray emission

TABLE 2

GAS CHARACTERISTICS

Model	kT (keV)	Central Density (cm^{-3})	Pressure 10″ from Core ($N\ m^{-2}$)	t_{cool} within Core Radius (yr)
β only	1	3.2×10^{-3}	8.8×10^{-13}	1.5×10^{10}
	5	3.5×10^{-3}	4.8×10^{-12}	3.0×10^{10}
	9	3.6×10^{-3}	8.8×10^{-12}	3.9×10^{10}
β and unresolved ..	1	5.6×10^{-4}	2.0×10^{-13}	8.4×10^{10}
	5	6.1×10^{-4}	1.1×10^{-12}	1.7×10^{11}
	9	6.2×10^{-4}	2.0×10^{-12}	2.2×10^{11}

in 3C 280 is from thermal gas of high temperature ($\gtrsim$ 9 keV; Table 2). In the preferred two-component fit to the X-rays, the gas pressure is insufficient to confine the lobes, as for some low-redshift radio galaxies (Miller et al. 1985). Overpressure inside the bow shock (e.g., Loken et al. 1992) may be required.

In summary, we find evidence for both unresolved and thermal X-ray emission in the powerful radio galaxy 3C 280. After comparing the unresolved X-ray and core radio emissions with those of radio-loud quasars of similar total (isotropic) power, we find (1) a correlation between the core X-ray and radio emission in core-dominated quasars, (2) 3C 280 lies on an extrapolation of the correlation, and (3) lobe-dominated quasars have X-ray emission in excess of the correlation. The inference from point (1), that the X-rays from core-dominated quasars are beamed, is supported by earlier work. Point (2) is most simply explained if the same core X-ray to radio relationship holds for radio galaxies as for core-dominated quasars; this will be tested by X-ray observations of other powerful radio galaxies. Point 3 suggests that lobe-dominated quasars contain an additional source of X-ray emission, possibly related to the nuclear X-ray emission in radio-quiet quasars. We infer that this compact X-ray component is obscured in radio galaxies, and dominated by beamed emission from the jet in core-dominated quasars.

We thank M. Birkinshaw for discussions and code used in the radial-profile fitting, and D. Harris, A. Marscher, and an anonymous referee for comments which helped to improve this manuscript. D. M. W. thanks the Caltech Astronomy Department for hospitality while this paper was being written. The work was funded by NASA grants NAG5-1706 and NAG5-1882, NASA contract NAS8-39073, and NSF grant AST 9117100.

REFERENCES

Antonucci, R. 1982, Nature, 299, 605
Arnaud, K. A., Fabian, A. C., Eales, S. A., Jones, C., & Forman, W. 1984, MNRAS, 211, 981
Barthel, P. D. 1989, ApJ, 336, 606
Birkinshaw, M., & Worrall, D. M. 1993, ApJ, 412, 568
Browne, I. W. A., & Murphy, D. W. 1987, MNRAS, 226, 601
Cavaliere, A., & Fusco-Femiano, R. 1978, A&A, 70, 677
Crawford, C. S., & Fabian, A. C. 1993, MNRAS, 260, L15
David, L. P., Slyz, A., Jones, C., Forman, W., Vritilek, S. D., & Arnaud, K. A. 1993, ApJ, 412, 479
Fabbiano, G., Miller, L., Trinchieri, G., Longair, M., & Elvis, M. 1984, ApJ, 277, 115
Feigelson, E. D., Isobe, T., & Kembhavi, A. 1984, AJ, 89, 1464
Gunn, J. E., Hoessel, J. G., Westphal, J. A., Perryman, M. A. C., & Longair, M. S. 1981, MNRAS, 194, 111
Hasinger, G., Turner, T. J., George, I. M., & Boese, G. 1992, NASA/GSFC/OGIP, Calibration Memo CAL/ROS/92-001
Hough, D. H., & Readhead, A. C. S. 1989, AJ, 98, 1208
Lawrence, C. R., et al. 1994, in preparation
Liu, R., Pooley, G., & Riley, J. M. 1992, MNRAS, 257, 545
Loken, C., Burns, J. O., Clarke, D. A., & Norman, M. L. 1992, ApJ, 392, 54
Marscher, A. P., Marshall, F. E., Mushotzky, R. F., Dent, W. A., Balonek, T. J., & Hartman, M. F. 1979, ApJ, 233, 498
Max-Planck Institute für Extraterrestriche Physik. 1992, *ROSAT* Newsletter, No. 10.
McCarthy, P. J., van Breugel, W., & Kapahi, V. K. 1991, ApJ, 371, 478
Miley, G. 1980, ARA&A, 18, 165
Miller, L., Longair, M. S., Fabbiano, G., Trinchieri, G., & Elvis, M. 1985, MNRAS, 215, 799
Pearson, T. J., & Readhead, A. C. S. 1988, ApJ, 328, 114
Pfeffermann, E., et al. 1987, in Soft X-ray Optics & Technology, Proc. SPIE, 733, 519
Raymond, J. C., & Smith, B. W. 1977, ApJS, 35, 419
Readhead, A. C. S. 1980, in IAU Symp. 92, Objects at High Redshift, ed. G. O. Abell & P. J. E. Peebles (Dordrecht: Reidel), 165
Readhead, A. C. S., Cohen, M. H., Pearson, T. J., & Wilkinson, P. N. 1978, Nature, 276, 768
Readhead, A. C. S., Hough, D. H., Ewing, M. S., Walker, R. C., & Romney, J. D. 1983, ApJ, 265, 107
Sarazin, C. L. 1986, Rev. Mod. Phys., 58, 1
Scheuer, P. A. G. 1987, in Superluminal Radio Sources, ed. J. A. Zensus & T. J. Pearson (Cambridge Univ. Press), 104
Stark, A. A., Gammie, C. F., Wilson, R. W., Bally, J., Linke, R. A., Heiles, C., & Hurwitz, M. 1992, ApJS, 79, 77
Trümper, J. 1983, Adv. Space. Res., 2, 241
Wilkes, B. J., Tananbaum, H., Worrall, D. M., Avni, Y., Oey, M. S., & Flanagan, J. 1994, ApJS, in press
Wilkinson, P. N., Polatidis, A. G., Readhead, A. C. S., Xu, W., & Pearson, T. J. 1993, in Sub-Arcsecond Radio Astronomy, ed. R. J. Davis & R. S. Booth (Cambridge Univ. Press), in press
Worrall, D. M., & Birkinshaw, M. 1994, ApJ, submitted
Worrall, D. M., Giommi, P., Tananbaum, H., & Zamorani, G. 1987, ApJ, 313, 596
Worrall, D. M., et al. 1992, in Data Analysis in Astronomy IV, ed. V. Di Gesu et al. (New York: Plenum), 145

A&A manuscript no.
(will be inserted by hand later)

Your thesaurus codes are:
03(11.02.1; 11.17.3; 13.18.2; 13.25.3)

ASTRONOMY
AND
ASTROPHYSICS
18.2.1994

X-ray Spectra of a Complete Sample of Extragalactic Core-dominated Radio Sources

H. Brunner[1], G. Lamer[1], D. M. Worrall[2], and R. Staubert[1]

[1] Astronomisches Institut der Universität Tübingen, Waldhäuserstr. 64, D-72076 Tübingen, Germany
[2] Harvard-Smithsonian Center for Astrophysics, 60 Garden Street, Cambridge, MA 02138, USA

Received December 23, 1993; accepted February 7, 1994

Abstract. We present ROSAT soft X-ray spectra for the members of a complete sample of 13 core-dominated, flat radio spectrum sources. The sample comprises all radio sources from a flux-limited radio catalog ($S_{5\mathrm{GHz}} > 1$ Jy; Kühr et al. 1981) which are north of $\delta = 70°$, at galactic latitudes $b > 10°$, and have a flat radio spectrum between 1.4 and 5 GHz ($\alpha_r < 0.5$; $f \sim \nu^{-\alpha}$). The sources have already undergone much study at radio and optical wavelengths and are classified in broad terms as quasars (8 sources) and BL Lac objects (5 sources). We find mean X-ray power-law energy indices of $\alpha_x = 0.59 \pm 0.19$ for the quasars and 1.36 ± 0.27 for the BL Lac objects (68 % confidence range for two parameters of interest as determined by a maximum likelihood method), supporting earlier *Einstein* Observatory results for heterogeneous samples of sources (Worrall and Wilkes 1990). A non-zero dispersion on α_x is found for both the quasars and the BL Lac objects.

The quasar X-ray spectra are harder than the interpolated spectral index between the optical and X-ray bands, α_{ox}, and they cluster tightly around $< \alpha_{ox} - \alpha_x > \simeq 0.6$. In contrast, the BL Lac objects give $< \alpha_{ox} - \alpha_x > \simeq 0$, but with a relatively large dispersion ($\sigma \sim 0.5$) which is similar to that on α_x. The BL Lac objects separate into a group of three sources with $\alpha_x < 1.0$ and two sources with $\alpha_x > 1.7$.

When we incorporate published radio, mm, and optical measurements and compare the X-ray and broad-band spectral indices α_x, α_{rx}, $\alpha_{mm,x}$, and α_{ox}, the most obvious difference between the quasar and BL Lac subsamples lies within the X-ray band. We have fitted the multi-wavelength data to inhomogeneous synchrotron-self-Compton models and find that, for the BL Lac objects with steep X-ray spectra, synchrotron emission can account for the radio to soft X-ray measurements, whereas the BL Lac objects with hard X-ray spectra and the quasars require significant Compton emission to model the spectral flattening indicated by $\alpha_x < \alpha_{ox}$.

Key words: BL Lacertae objects – quasars – radio continuum – X-rays

Send offprint requests to: H. Brunner

1. Introduction

A link between the X-ray and the radio emission in radio-loud quasars has long been established. Several authors (e.g., Kembhavi, Feigelson and Singh 1987; Worrall et al. 1987; Browne and Murphy 1987) report correlations between the radio and X-ray emissions in samples of quasars observed with the *Einstein* Observatory Imaging Proportional Counter (IPC), the dependence being more pronounced in compact flat radio spectrum quasars than those with extended steep-spectrum components. The X-ray spectral indices are also found to be linked with the radio emission. Wilkes and Elvis (1987) were the first to report flatter X-ray power-law indices for radio-loud than radio-quiet quasars, and Canizares and White (1989) and Brunner et al. (1989) found that flat radio spectrum and steep radio spectrum quasars have different X-ray slopes. A comparison of the mean X-ray spectral index between core-dominated quasars and BL Lac objects revealed a striking difference between these two classes also (Worrall and Wilkes 1990). Spectral surveys performed with X-ray detectors sensitive in different energy ranges now support (1) an increase in diversity of spectral index as one moves to lower X-ray energies (< 1 keV) and (2) a general trend of spectral steepening below 1 keV for quasars (e.g., with *Einstein* IPC: Masnou et al. 1992; EXOSAT: Comastri et al. 1992; Ginga: Williams et al. 1992; ROSAT PSPC: Brunner et al. 1991 and 1992, Walter and Fink 1993, Brinkmann et al. 1993).

The correlation between the radio and X-ray emission can be understood in terms of different X-ray components being related to different parts of the compact and possibly also to the extended radio emission, their relative strength being governed by effects of relativistic beaming and inclination (e.g. Browne and Murphy 1987). For both core-dominated quasars and BL Lac objects, the link between X-ray and radio emission is most often discussed in the framework of relativistically beamed plasma jet models. The radio to soft X-ray continuum is then relativistically beamed synchrotron radiation, where, to first approximation, either a homogeneous synchrotron source

is assumed, or the magnetic field strength and the electron density are parameterized as powers of the radial distance along the jet axis. Lorentz factors of the bulk relativistic motion are thought to be in the range from 1 to ~ 10, with some evidence that the X-ray radiation in its entirety is less beamed than the radio emission. Beaming factors of BL Lac objects are thought to be somewhat lower and more widely scattered than those of core-dominated quasars (Ghisellini et al. 1993).

The observed difference in X-ray power-law spectral index between core-dominated quasars and BL Lac objects may be due in part to the different distributions of redshift and beaming factor of the two classes, with different physical components (e.g., Compton vs. synchrotron) dominating in each case. The spectral steepening and increased dispersion in spectral index towards low X-ray energies can be accommodated in this picture by assuming that the steep component at low X-ray energies is due to synchrotron emission, and that the hard component is from Compton scattering which sets in at different energies depending on redshift, beaming factor, and perhaps other source characteristics. Further discussion of this model appears later in this paper.

The study presented here is unique in that for the first time results are obtained for a complete, flux-limited sample of core-dominated radio sources, with sufficient integration time to determine X-ray spectra. Our sample is a complete subset of 13 sources from the S5 radio sample (see below), and, as such, a wide range of data from other spectral bands is available, including VLBI coverage for all sample members (e.g. Eckart et al. 1987, Witzel et al. 1988, Chini et al. 1988, Pearson and Readhead 1988). We present the ROSAT PSPC spectral data for each source (section 3) as well as a re-analysis of data obtained with the *Einstein* Observatory (section 4) and EXOSAT (section 5) for some of the sample members. The mean spectral characteristics of the quasar and BL Lac subsamples are determined (section 7) and discussed both in conjunction with the available broad-band spectral data (section 8) and with X-ray results obtained earlier for incomplete samples of quasars and BL Lac objects (section 9). We interpret the X-ray and broad-band data in the context of symmetric and inhomogeneous synchrotron self-Compton models (section 10): Beaming factors and jet-model parameters are presented.

2. Description of the sample

The S5 sample consists of all radio sources north of declination $\delta = 70°$, with galactic latitudes $> 10°$, and which are brighter than 1 Jy at 5 GHz (Kühr et al. 1981). It is the northernmost section of the *Strong Source (S) Surveys* undertaken by NRAO and MPIfR at frequencies of 1.4 and 5 GHz. Here we present ROSAT X-ray spectra for the complete subset of 13 flat radio spectrum sources with $\alpha_r < 0.5$ ($f \sim \nu^{-\alpha}$) from the S5 sample. The sources have already been widely studied at radio and optical wavelengths and they have been classified in broad terms as quasars (8 sources) and BL Lac objects (5 sources). 8 of the 13 sources have a 5 GHz flux density > 1.3 Jy and are also in the Pearson and Readhead (1988) VLBI survey. Table 1 gives redshifts. Table 9, later, gives visual magnitudes and total radio flux densities. A comparison with VLBI flux densities, Table 12, shows that all the sources are core-dominated with $> 40\%$ of their flux density at 5 GHz within a parsec-scale emission region. A summary of source properties follows (taken from Witzel et al. (1988) where not mentioned otherwise):

Table 1. Type and redshift of sample members

target	type	redshift	
Quasars			
0016+731	Q (3)	1.781	(1)
0153+744	Q (3)	2.338	(1)
0212+735	Q (3)	2.367	(1)
0615+820	Q (4)	0.71	(3)
0836+710	Q (3)	2.17	(4)
1039+811	Q (4)	1.26	(3)
1150+812	Q (4)	1.25	(3)
1928+738	Q (3)	0.302	(1)
BL Lacs			
0454+844	BL (2)	0.112	(5)
0716+714	BL (2)	> 0.3	(6)
1749+701	BL (2)	0.770	(2)
1803+784	BL (2)	0.6797	(7)
2007+777	BL (2)	0.342	(2)

1: Lawrence et al. 1986 2: Stickel et al. 1989 3: Eckart et al. 1986 4: Hewitt and Burbidge 1987 5: Lawrence 1992 6: Wagner et al. 1990 and Wagner 1993 7: Pearson and Readhead 1988 and Lawrence 1992

0016+731: The source has a very compact VLBI structure. A single component contains 100 % of flux density at 18 cm. Eckart et al. (1987) find indications that the source is increasingly resolved at higher frequencies.

0153+744: This source has a double VLBI structure with weak optically-thin emission observed in a curved structure between the components (Hummel et al. 1988). Upper limits to the proper motion show the source to be subluminal for $H_0 = 100$ km s^{-1} Mpc^{-1} (Table 11). It is the only sample member for which the 5 GHz to 230 GHz spectral index is steeper than 0.4 (Chini et al. 1988).

0212+735: The source displays a core-jet VLBI structure with measured superluminal motion. The optical emission lines are relatively weak and variable and the optical polarization is relatively high and also variable (Biermann et al. 1981, Impey et al. 1991). The source is classified as one of two HPQ/OVVs (with 0836+710) among the quasars which otherwise have low optical polarization (except 0615+832, 1039+811, and 1150+812 for which no polarization measurements are available). When the source was first observed optically, no emission lines were seen (Krichbaum 1992). This may be an example of a source which is classified as either a BL Lac or a quasar depending on when it is viewed. Note that for this source, two different X-ray spectral shapes have been observed (see below).

Table 2. Log of ROSAT PSPC observations

target	ROR[a] number	observation date	livetime [ks]	off ax.[b] [arcmin]	source counts 0.1–2.4 keV
Quasars					
0016+731	700494	Mar 11/12 92	6.01	0.20	54 ± 9
0153+744	700138	Mar 16/18 91	2.94	0.22	30 ± 7
	700138	Mar 11 92	4.93	0.22	59 ± 8
0153+744	700495	Mar 11 92	8.29	17.93	50 ± 7
0212+735	700139	Feb 16/18 91	7.21	0.31	308 ± 18
0615+820	700492	Feb 22/23 93	7.40	0.05	79 ± 9
0615+820	701060	Mar 11 93	3.92	0.05	64 ± 10
0836+710	700493	Mar 23/26 92	6.99	0.14	5365 ± 75
0836+710	701061	Nov 2/3 92	5.03	0.23	1904 ± 44
1039+811	700141	Mar 17/18 91	6.57	0.17	500 ± 32
1150+812	700496	Apr 8 92/	2.93	0.19	58 ± 9
1150+812	700496	May 7/10 92	5.65	0.19	172 ± 14
1150+812	701059	Oct 29/30 92	9.50	0.36	241 ± 17
1928+738	700142	Mar 14/15 91	8.45	0.09	2314 ± 48
BL Lacs					
0454+844	700140	Apr 4/ 6 91	3.36	-[c]	-[c]
0454+844	701058	Sept 25/26 92	8.05	0.38	36 ± 6
	701058	Aug 17/18, 93	6.81	0.35	27 ± 5
0716+714	700210	Mar 8/11 91	21.04	0.09	16236 ± 128
1749+701	RASS[d]	Sep 27/28 90	10.5	-	410
1803+784	700497	Apr 7 92	6.91	0.36	539 ± 24
2007+777	700498	Dec 11/12 91	5.37	5.62	227 ± 16
	700498	May 17 92	4.16	5.74	216 ± 15

[a] ROSAT observation request number.
[b] Angular distance of source centroid from telescope axis.
[c] Source not detected.
[d] ROSAT All-Sky Survey.

0454+844: Compact VLBI structure. Superluminal motion has been measured. Source is declining in radio flux density, and values in this paper may overestimate the radio strength at the time of the ROSAT measurement.

0615+820: Very compact VLBI source with upper limit to superluminal motion.

0716+714: Very compact VLBI structure with upper limit to the superluminal motion. This is one of the two most interesting sources for intraday variability (IDV; with 0917+62; Krichbaum et al. 1992). Unlike 0917+62, a quasar, the radio strength and polarization variations are correlated (Wegner et al. 1993). This source exhibited the best example of correlated radio and optical variability in February 1990 (Quirrenbach et al. 1991), arguing against an extrinsic cause for the variability. The ROSAT observation, which was between optical flares, shows high-amplitude variability whose relation to the radio variability is unclear (Witzel et al. 1993; Wagner et al. 1993). Gamma-ray emission has been detected with EGRET (Michelson et al. 1992).

0836+710: The source shows a one-sided VLBI jet with superluminal motion and stationary components. There is a co-aligned one-sided arcsec jet (O'Dea et al. 1991). An optical flare and optical polarization has been observed and the source is classifed as an HPQ/OVV (von Linde et al. 1993, Wagner 1994). Gamma-ray emission has been detected with EGRET (Thompson et al. 1993). Note that 0836+710 and 0716+714, the two sample members from which Gamma-ray emission has been detected, have flatter overall multi-wavelength spectra ($\alpha_{rx} < 0.8$; see Tab. 9) than any of the other sample members. 0836+710 also displays the flattest X-ray spectrum (see below).

1039+811: The source displays a compact VLBI structure. An upper limit to superluminal motion is reported.

1150+812: The source has a compact structure with measured superluminal motion. Many instances of IDV have been observed (Krichbaum et al. 1992).

1749+701: This is a compact VLBI source with superluminal motions measured. It was the first observed good case of IDV (Heeschen et al. 1987).

1803+784: For this compact VLBI source, superluminal motion and stationary components are reported. IDV is observed.

1928+738: Compact VLBI source with superluminal motion. The source may be located in a cluster of galaxies (Wagner 1993), perhaps indicating multiple X-ray emission components and accounting for the relatively poor fit of the

X-ray data to a single power-law with Galactic absorption (see Fig. 1).

2007+777: Compact VLBI source with superluminal motion. IDV is reported by Krichbaum et al. (1992).

3. ROSAT measurements

3.1. Observations and analysis methods

The 13 sample sources have been measured with the ROSAT PSPC. Eleven were observed by us for this project during the A01 through A03 pointed phases of the mission. Integration times were from 6 to 18 ks, and between $\sim$ 50 and $\sim$ 5000 net counts per target were obtained. Of the remaining two targets, 0716+714 was observed for 21 ks as part of a separate program (Witzel et al. 1993); although the source is included in our analysis of sample properties, detailed results are presented elsewhere (Wagner et al. 1993). 1749+701 is located close to the ecliptic pole and thus has a total integration time of 10.5 ks in the ROSAT All-Sky Survey (RASS; Voges 1992). The spectral results have been reported by Fink et al. (1992) and are included in our analysis. The weakest source in our sample, 0454+844, was found to be only 48″ away from a relatively bright X-ray source ($\sim 5\times$ count rate of target). We therefore suspect that previous reports of X-ray emission from 0454+844 may be due to a mis-identification.

The ROSAT data-analysis was performed using the EXSAS software (*EX*tended *S*cientific *A*nalysis *S*ystem; export version January 93; Zimmermann et al. 1993). Source counts were generally extracted from a circle of radius 100″, and the background was determined from an annulus with inner and outer radii of 150″ and 200″, respectively. Due to the low detector background of the ROSAT PSPC (total background $\sim$ 10 counts per source area per 8 ks) the spectral results are relatively insensitive to the size of the on-source and background areas. Corrections for telescope vignetting, dead time, and incomplete coverage of the point spread function were applied using the EXSAS correction package. The spectra were fit over the energy range 0.10 to 2.4 keV. The data were binned so that the significance of each spectral bin was 9σ for the brighter sources and 5σ for the weaker sources. Uncorrected background-subtracted counts (0.1 – 2.4 keV) are given in Table 2.

We have tested whether our data might be affected by *ghost images* (deviations from the model point spread function resulting from the low number of secondary electrons within the PSPC for photon energies < 0.2 keV) by extracting the source counts from areas of varying size; we do not find any significant change of the resulting best-fit spectral parameters and conclude that our data are largely unaffected by this problem. This may in part be attributed to the fact that, for several sample members, the line of sight absorption due to hydrogen column density within our galaxy is sufficient to absorb much of the flux below 0.2 keV.

3.2. Variability analysis

Except for 0716+716, none of the sources exhibits a significant difference in mean flux between the first and second halves of the pointed observations. Table 3 (last column) lists the upper limits (3σ) for this test.

We have also performed a χ^2 test for variability of sources with sufficient counts, using the bin-widths given in Table 3. Only 0716+714 shows significant variability (Witzel et al. 1993), which is discussed in detail elsewhere (Wagner et al. 1993).

We have compared the net count rates between individual observations where detections from more than one observation (RASS or pointed) were available (see Table 4). The RASS counting rates used the output from the first analysis of the survey data with the Standard Analysis Software System (SASS, Voges 1992; see also Brunner et al. 1992). We find no significant variability ($> 3\sigma$) between observations except for the following two sources:

Table 3. χ^2 values and upper limits for variability amplitudes (ROSAT pointed observations)

target	bin width [s]	red. χ^2 (d.o.f.)	amplitude[a] [%]
Quasars			
0016+731			< 138 %
0153+744[b]			< 242 %
0153+744[c]			< 81 %
0212+735	300	1.23 (20)	< 41 %
0615+820[d]			< 102 %
0615+820[e]			< 120 %
0836+710[f]	100	1.03 (59)	< 9 %
0836+710[g]	100	1.23 (47)	< 15 %
1039+811	300	1.06 (19)	< 31 %
1150+812[h]	400	1.25 (12)	< 59 %
1150+812[i]	400	1.47 (16)	< 48 %
1928+738	200	1.06 (37)	< 13 %
BL Lacs			
0454+844[k]			< 200 %
0454+844[l]			< 273 %
0716+714	50	55.2 (405)	–[m]
1803+784	400	1.70 (11)	< 30 %
2007+777	200	1.27 (41)	< 33 %

[a] 3 σ upper limit for the amount of variability between the first and second half of the observation.
[b] March 91 [c] March 92 [d] Feb. 93 [e] March 93 [f] March 92 [g] Nov. 92
[h] May 92 [i] Oct. 92 [k] Sept 92 [l] Aug. 93
[m] Data are sensitive to variability of > 5% which has been detected (Witzel et al. 1993).

0716+714: In the pointed observation the source was brighter by a factor of three, on average, than during the RASS observation.

0836+710: The ROSAT counting rate decreased by a factor of two between March 26, 1992 and Nov. 2, 1992. A similar

Table 4. Source count rates (0.07–2.4 keV) in pointed (P) and survey (S) observations (corrected for telescope vignetting; taken from maximum-likelihood analysis of SASS). Sources only detected in one (either survey or pointing) observation are not listed.

target	P/S	date of obs.	count rate [cts/s]
Quasars			
0153+744	P	March 16/18 91	0.0082 ± 0.0017
	P	March 11 92	0.0095 ± 0.0018
0212+735	S	Aug. 16 90	0.046 ± 0.017
	P	Feb. 16/18 91	0.043 ± 0.002
0615+820	P	Feb. 22/23 93	0.017 ± 0.001
	P	Mar 11 93	0.014 ± 0.002
0836+710	S	Oct. 1 90	0.802 ± 0.053
	P	March 23/26 92	0.755 ± 0.011
	P	Nov. 2/3 92	0.379 ± 0.009
1039+811	S	Oct. 1 90	0.070 ± 0.012
	P	March 17/18 91	0.076 ± 0.004
1150+812	P	Apr 8 92 /	0.020 ± 0.003
	P	May 7/10 92	0.030 ± 0.002
	P	Oct. 29/30 92	0.025 ± 0.002
BL Lacs			
0454+844	P	Sep. 25/26 92	0.0052 ± 0.0009
	P	Aug. 17/18 93	0.0050 ± 0.0009
0716+714	S	Sept. 22 90	0.276 ± 0.031
	P	Mar. 8/11 91	0.772 ± 0.006
1803+784	S	Sept. 11 90	0.065 ± 0.011
	P	April 7 92	0.078 ± 0.004
1928+738	S	Aug. 5 90	0.255 ± 0.013
	P	March 14/15 91	0.277 ± 0.006
2007+777	S	Aug. 14 90	0.034 ± 0.009
	P	Dec 11/12 91	0.042 ± 0.003
	P	May 17 92	0.052 ± 0.004

decrease in optical flux was seen in almost simultaneous measurements (Wagner 1993). Earlier, in Oct. 1990, the RASS observed an X-ray flux similar to the (higher) value of March 1992. Both the EGRET observation (Jan. 1992; Thompson et al. 1993) and an optical flare (Feb. 16, 1992; von Linde et al. 1993) took place within two months of the March 1992 ROSAT observation. Optical polarization was observed at the time of the optical flare (Wagner 1994) while only marginal polarization was found in a previous measurement (Impey et al. 1991).

Power-law spectral index variability will be discussed in the next section.

3.3. Spectral analysis

Power-law spectral fits with absorption represented by the Galactic column density of $N_{\rm H}$ (Stark et al. 1992) are acceptable for most of the observations. For those sources where a sufficient number of counts (> 400) was collected, we have also performed power-law fits with $N_{\rm H}$ as a free parameter. Results for all sample members are given in Table 5, and error contour plots for cases where $N_{\rm H}$ was a free parameter are shown in Fig. 1. Note that in two cases (0454+844 and 1150+812) individual observations were combined to yield the required number of counts for performing meaningful spectral fits.

In the case of 0716+714, fits using the latest available version of the detector response matrix (nr. 36) lead to statistically unacceptable best-fit reduced χ^2 values, both for the fixed and the free $N_{\rm H}$ power-law fits. Acceptable best-fit χ^2 values are achieved, however, using an earlier version of the detector response matrix (nr. 6; August 1992). The older response matrix may be more appropriate for observations performed before fall 1991 (as is the case for 0716+714), when a different gain setting of the PSPC detector was used (Hasinger 1993). Alternatively, the addition of 4 % systematic errors in our spectral fits will also reduce the best fit reduced χ^2, achieved using response matrix 36, to acceptable values. While power-law indices determined using the old response matrix tend to be slightly lower ($\Delta\alpha_x \leq 0.1$), the change in spectral parameters when using both detector response matrices is within statistical errors for all sample members. We have used response matrix nr. 6 for all observations performed before fall 1991 and response matrix nr. 36 for all later observations.

In the first observation of 1150+812 the fixed $N_{\rm H}$ fit gives a χ^2 which is only marginally acceptable. An improved fit can be achieved when substantial amounts of excess absorption ($\sim 2 \times 10^{21}$ cm^{-2}) are permitted. The free $N_{\rm H}$ fit performed on the combined data set (see Table 2) confirms this result.

In the case of 0212+735 an anomalously hard X-ray spectrum is observed (see also next section on *Einstein* IPC data analysis). Note that the ROSAT spectrum can also be fit by doubling the Galactic absorption given by Stark et al. (1992) and fixing the power-law index at a more standard value ($\alpha_x = 0.4$) for core-dominated quasars.

All our free-$N_{\rm H}$ power-law fits are consistent with the Galactic value at the 90% confidence level for two interesting parameters (see Fig. 1). Of the four *quasars* where free $N_{\rm H}$ fits could be performed, three (at $z = 0.302, 1.25$, and 2.17) show a slight tendency to prefer excess $N_{\rm H}$, while the fourth ($z = 1.26$) fits a slight deficit of $N_{\rm H}$ with respect to the Galactic value. In conjunction with the spectral results on 0212+735, above, there may be a marginal overall trend towards excess $N_{\rm H}$ in high-redshift quasars in our sample. Results are inconclusive, however, and, due to poor statistics, do not provide additional support to the report by Elvis et al. (1994) that quasars of $z > 1$ exhibit absorption in excess of the Galactic column density.

Some of the absorbing material in the region of the north celestial pole is known to be in the form of Galactic molecular clouds (Polaris flare, Cepheus flare; Grenier et al. 1989, Heithausen and Thaddeus 1990, Heithausen et al. 1993). We have checked whether significant excess absorption in the soft X-ray range is to be expected for any of the sample members due to these clouds. For two of the sources, 0153+744 and 0212+735, a velocity-integrated CO emission of ~ 2 K km s^{-1} has been measured, while for 0016+731 an upper limit of the same order can be given (Grenier et al. 1989, Liszt and Wilson 1993). This corresponds to an equivalent H_2 column density of $4 - 8 \times 10^{20}$ cm^{-2} (Scoville and Sanders 1987), not included in the H I

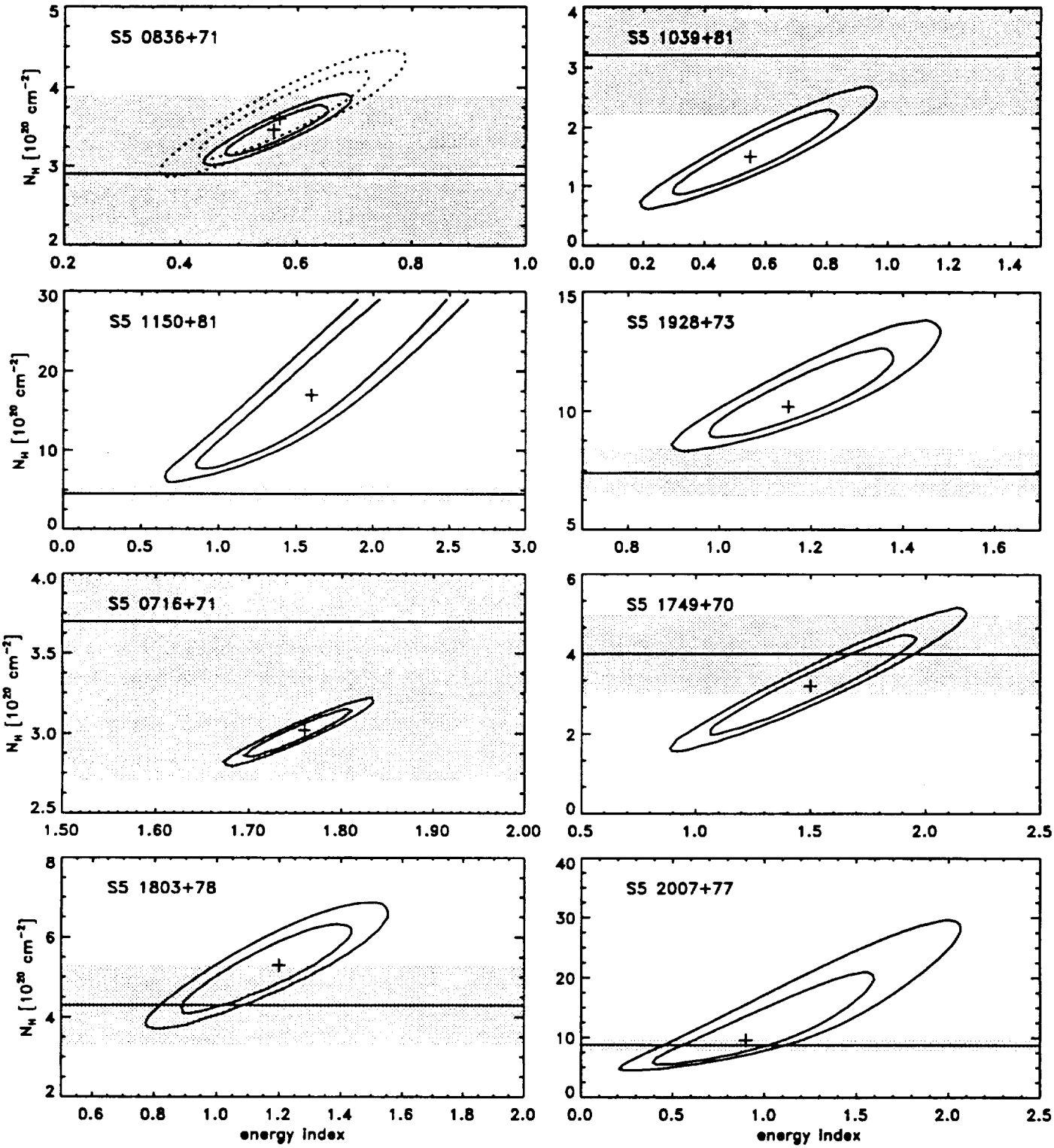

Fig. 1. Energy index vs. $N_{\rm H}$ error contours for ROSAT targets where more than 400 source counts were observed. 68% and 90% error contours for two interesting parameters are presented. The two observations of 0836+710 were treated separately (dashed contours: second observation). The horizontal lines mark Galactic $N_{\rm H}$; shaded regions indicate uncertainties of $\pm 10^{20}$ atoms cm^{-2} (Elvis et al. 1986).

Table 5. ROSAT spectral parameters

target	ROR number	N_H $[10^{20} cm^{-2}]$[a]	1 keV flux density μJy[a]	power-law energy index[a]	red. χ^2 (dof)
		Galactic N_H			
Quasars					
0016+731	700494	22.0	$0.043^{+0.015}_{-0.017}$	$0.00^{+1.25}_{-0.58}$	1.08 (2)
0153+744	700138	24.1	$0.059^{+0.010}_{-0.012}$	$0.35^{+0.64}_{-0.65}$	0.29 (2)
0212+735	700139	24.7	$0.200^{+0.028}_{-0.028}$	$-0.56^{+0.39}_{-0.41}$	1.10 (8)
0615+820	700492	5.2	$0.036^{+0.007}_{-0.007}$	$1.02^{+0.36}_{-0.36}$	1.01 (3)
0615+820	701060	5.2	$0.047^{+0.010}_{-0.014}$	$1.49^{+0.40}_{-0.49}$	2.55 (2)
0836+710	700493	2.9	$2.305^{+0.050}_{-0.055}$	$0.42^{+0.03}_{-0.04}$	1.12 (42)
0836+710	701061	2.9	$1.165^{+0.039}_{-0.045}$	$0.39^{+0.04}_{-0.06}$	1.16 (16)
1039+811	700141	3.2	$0.184^{+0.016}_{-0.016}$	$1.09^{+0.13}_{-0.13}$	1.59 (13)
1150+812	700496	4.5	$0.087^{+0.009}_{-0.010}$	$0.55^{+0.21}_{-0.25}$	2.58 (5)
1150+812	701059	4.5	$0.087^{+0.009}_{-0.009}$	$0.41^{+0.19}_{-0.29}$	1.08 (5)
1928+738	700142	7.4	$1.052^{+0.033}_{-0.034}$	$0.80^{+0.08}_{-0.08}$	1.12 (18)
BL Lacs					
0454+844	[b]	5.6	$0.0168^{+0.0033}_{-0.0034}$	$1.43^{+0.52}_{-0.47}$	0.69 (4)
0716+714	700210	3.7	$1.269^{+0.025}_{-0.026}$	$2.01^{+0.02}_{-0.02}$	1.20 (54)
1749+701[c]	–	4.0	$0.140^{+0.017}_{-0.016}$	$1.78^{+0.14}_{-0.14}$	0.59 (10)
1803+784	700497	4.3	$0.226^{+0.019}_{-0.016}$	$0.97^{+0.23}_{-0.12}$	0.91 (14)
2007+777[d]	700498	8.8	$0.181^{+0.020}_{-0.019}$	$0.84^{+0.31}_{-0.50}$	0.16 (4)
2007+777[e]	700498	8.8	$0.218^{+0.023}_{-0.023}$	$0.76^{+0.37}_{-0.38}$	0.62 (3)
		N_H fitted			
Quasars					
0836+710	700493	$3.5^{+0.4}_{-0.4}$	$2.370^{+0.098}_{-0.098}$	$0.57^{+0.11}_{-0.11}$	1.01 (41)
0836+710	701061	$3.6^{+0.8}_{-0.6}$	$1.208^{+0.086}_{-0.086}$	$0.57^{+0.19}_{-0.18}$	1.00 (15)
1039+811	700141	$1.5^{+1.2}_{-0.7}$	$0.175^{+0.022}_{-0.021}$	$0.56^{+0.41}_{-0.30}$	0.99 (12)
1150+812	[f]	$20.7^{+38.9}_{-12.7}$	$0.155^{+0.200}_{-0.200}$	$2.85^{+0.93}_{-1.87}$	0.88 (11)
1928+738	700142	$10.5^{+2.9}_{-2.0}$	$1.180^{+0.279}_{-0.282}$	$1.17^{+0.28}_{-0.22}$	0.55 (17)
BL Lacs					
0716+714	700210	$3.0^{+0.2}_{-0.2}$	$1.301^{+0.031}_{-0.031}$	$1.75^{+0.07}_{-0.07}$	1.96 (53)
1749+701[c]	-	$3.1^{+1.7}_{-1.4}$	$0.143^{+0.019}_{-0.019}$	$1.49^{+0.62}_{-0.53}$	0.56 (9)
1803+784	700497	$5.2^{+1.4}_{-1.3}$	$0.235^{+0.025}_{-0.025}$	$1.16^{+0.34}_{-0.34}$	0.87 (13)
2007+777	700498	$9.5^{+16.5}_{-4.0}$	$0.198^{+0.164}_{-0.159}$	$0.86^{+0.99}_{-0.56}$	0.55 (11)

[a] Errors are $\chi^2_{min} + 2.3$ for fixed N_H fits; $\chi^2_{min} + 3.53$ for free N_H fits.
[b] Combined fit of RORs 700140 and 701058.
[c] Results from RASS.
[d] Dec. 11/12, 1991.
[e] May 17, 1992.
[f] Combined fit of RORs 700496 and 701059.

column densities determined from 21 cm radio measurements (Stark et al. 1992) which were used in our fixed N_H spectral fits. The amount of low-energy X-ray absorption (mainly due to He I) may thus be underestimated by up to 40 % in these sources. This may be sufficient to change the anomalously hard X-ray spectral index observed in 0212+735 to be consistent with a spectral index as expected for core dominated quasars. None of the other sample members lies in the direction of any known molecular clouds (Heithausen et al. 1993).

No significant spectral-index variability is found with ROSAT between any combination of RASS and pointed observations for a given target, and no spectral-index variability was observed within an individual observation. (See previous section for comments on flux variability).

Fig. 2 plots the individual ROSAT power-law spectral indices together with broad-band spectral indices (see section 8). The plot shows the values of α_x which are used in the composite analysis presented later in section 7. A weighted mean of the power-law indices was taken where multiple ROSAT observations were available.

4. *Einstein* Observatory measurements

4.1. Data analysis and results

A number of S5 sample members were previously observed with the *Einstein* Observatory IPC (Table 6) in pointed observations. Biermann et al. (1992) present flux densities, assuming

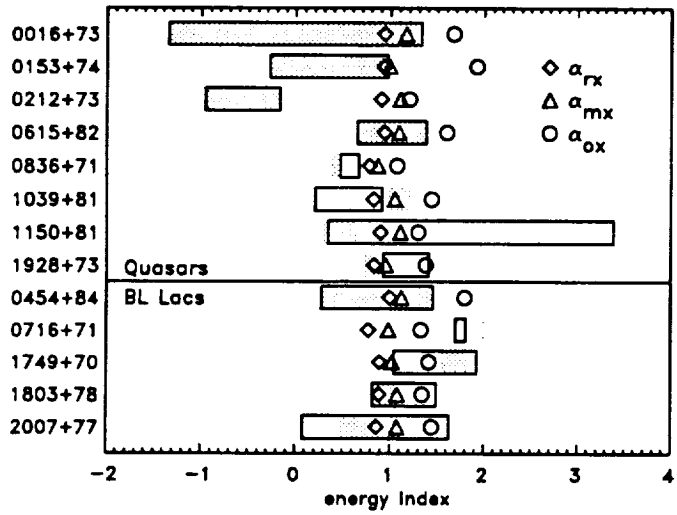

Fig. 2. ROSAT energy indices and 1 σ errors from fits with fixed (shaded bars) and free (open bars) N_H plotted together with three broad-band spectral indices α_{rx} (diamonds), $\alpha_{230GHz,x}$ (triangles), and α_{ox} (squares). See text for details on broad-band spectral indices.

Table 6. Log of *Einstein* observatory IPC observations

target	sequence number	observation date	livetime [ks]	net counts[a] 0.1–3.5 keV
Quasars				
0016+731	7583	Aug 24, '80	2.05	23 ± 9[b]
0212+735	7584	Mar 13, '80	2.97	197 ± 16
	10235	Jan 16, '81	9.06	483 ± 27
1928+738	7589	Apr 5, '80	2.27	246 ± 20
BL Lacs				
0454+844	7585	Mar 12, '80	1.70	20 ± 8[b]
0716+714	5120	Oct 19, '79/ Mar 9, '80	2.82	204 ± 17[c]
1749+701	2720	Jul 22, '79	1.81	88 ± 11
	8846	May 27, '80	0.83	38 ± 7[b]
1803+784	5121	Oct 30, '79	2.45	120 ± 14
2007+777	5122	Oct 20, '79	3.11	119 ± 16

[a] From a circle around source centroid of radius 3′, with background from an annulus of radii 5′ and 6′. Energy band is approximate. Before vignetting and scattering corrections applied.
[b] Radio position used for centroid of X-ray emission.
[c] Position angles 160° – 230° excluded from background to prevent contamination by probable weak source.

a power-law spectrum of slope $\alpha = 0.5$ and absorption given by the Galactic column density of HI. In addition, three of the sources, 0212+735, 0836+710, and 1928+738, were detected in the IPC Slew Survey (Elvis et al. 1992). In order to compare with the ROSAT measurements, we have re-fitted the pointed data allowing the power-law spectral slope to vary. We extracted the pulse-height distributions from the *Einstein* Catalogue of IPC event files (as published on CD-ROM in June 1992) and analyzed them using the Post-Reduction Off-line Software (PROS; Worrall et al. 1992) in the Image Reduction and Analysis Facility (IRAF) environment. Source counts were extracted from a circle of radius 3′, and the background was taken from an annulus of radii 5′ – 6′.

An exception to our analysis procedure was made for the source 1928 + 738. The event file for IPC sequence number 7589 has only 13 s of data because a good spacecraft aspect solution was not available for most of the observation. This observation was re-processed without correcting for spacecraft motion. Since the resulting image shows the photons to be well clustered within the region of the point-source response, we conclude that the spacecraft was stable during the observation despite the lack of ability to construct an aspect solution for most of the time, and our analysis used the re-processed event file.

Spectral results are given in Table 7. The net counts are too small (Table 6) to warrant fits where N_H is free to vary. However, for 1928 + 738, where the ROSAT data prefer an absorption slightly in excess of the Galactic value, we present an additional fit for an N_H more representative of the ROSAT best-fit value.

4.2. *Comparison with ROSAT*

The *Einstein* Observatory IPC spectral parameters are consistent with the ROSAT results to within 90% confidence for most sample members. Exceptions are listed below:

0212+735 was observed twice with the IPC. On the second occasion the source exhibited a hard X-ray spectrum, of similar slope and normalization to that measured with the ROSAT PSPC. However, nine months earlier the source was brighter and the spectrum was similar to the average for the quasar subsample.

0716+714 exhibited a 1 keV flux-density with the IPC which agrees with that measured in the RASS and which is a factor of three lower than the pointed ROSAT measurement. The IPC spectral index is flatter than that measured with ROSAT. Since no spectral-index variability has been found with ROSAT (Wagner et al. 1993), and the response of the IPC is biased towards energies higher than that of the PSPC, it is possible that this source exhibits spectral curvature, flattening to higher energy.

1928+738 was brighter when observed with ROSAT (and EXOSAT, see below) than during the earlier IPC observation. The spectral index is poorly constrained with the IPC; the brightening corresponds to a ~ 50% increase in 1 keV flux density, assuming a constant spectral index.

5. EXOSAT measurements

Four objects from the sample (0615+821, 1150+812, 1803+784 and 1928+738) were previously observed with EXOSAT. Flux densities (assuming a power-law spectrum of slope $\alpha = 0.5$

Table 7. *Einstein* Observatory IPC spectral parameters

target	sequence number	N_H [$10^{20} cm^{-2}$]	1 kev flux density μJy[a]	power-law energy index[a]	red. χ^2 (dof)
		Galactic N_H			
Quasars					
0016+731	7583	22.0	$0.11^{+0.08}_{-0.08}$	> 0.70	1.01 (7)
0212+735	7584	24.7	$0.51^{+0.12}_{-0.12}$	$0.37^{+0.45}_{-0.47}$	1.26 (8)
	10235[b]		$0.23^{+0.06}_{-0.06}$	$-0.56^{+0.34}_{-0.36}$	1.51 (7)
1928+738	7589[c]	7.4	$0.65^{+0.11}_{-0.11}$	$0.50^{+0.35}_{-0.37}$	0.90 (8)
BL Lacs					
0454+844[d]	7585	5.6	$0.06^{+0.09}_{-0.06}$	> 0.75	1.37 (8)
0716+714	5120	3.7	$0.37^{+0.06}_{-0.04}$	$0.56^{+0.30}_{-0.34}$	1.58 (8)
1749+701	2720[e]	4.0	$0.25^{+0.05}_{-0.06}$	$1.01^{+0.72}_{-0.91}$	1.65 (8)
	8846[e]		$0.21^{+0.08}_{-0.11}$	$1.45^{+1.11}_{-1.05}$	1.35 (7)
1803+784	5121	4.3	$0.28^{+0.05}_{-0.06}$	$1.06^{+0.54}_{-0.57}$	1.14 (8)
2007+777	5122	8.8	$0.26^{+0.07}_{-0.07}$	$0.81^{+0.64}_{-0.66}$	1.39 (8)
		PSPC best-fit N_H			
1928+738	7589	11.5	$0.76^{+0.12}_{-0.16}$	$0.70^{+0.40}_{-0.40}$	0.59 (7)

[a] 1 σ errors for 2 interesting parameters (normalization and energy index). $\chi^2_{min} + 2.3$.
[b] Unusually low gain. BAL $\sim$ 12. Spectral index anomalously flat.
[c] No aspect solution for all but 13 s of data, although image indicates that aspect was relatively stable. Applicable gain known only for 13 s of stable aspect. Additional uncertainties should be added to the spectral parameters due to uncertainties in the IPC gain.
[d] May be mis-identification with X-ray brighter source 48″ away (see section 3.1).
[e] Source not in center of field. Additional uncertainties should be added to the spectral parameters due to uncertainty in the IPC off-axis gain.

and absorption given by the Galactic column density) are given by Biermann et al. (1992). Here, we have fitted the data which are available from the ESTEC EXOSAT data base using the XSPEC spectral-fitting program.

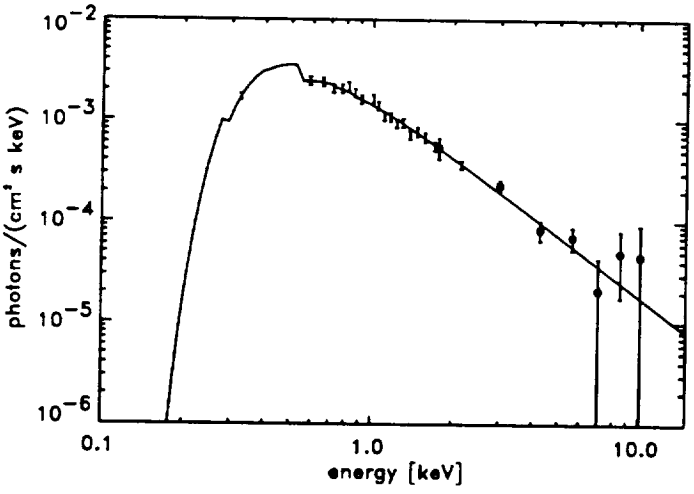

Fig. 3. Joint ROSAT (error bars only) and EXOSAT (full dots) spectral fit for 1928+738. See text for details.

Only 1928+738, which was observed multiple times, permitted the determination of well-defined spectral parameters. Power-law fits to the LE and ME data, with N_H fixed at the Galactic value, are listed in Table 8 for each of the four individual observations. Results which are in general agreement with ours have been presented by Ghosh and Soundararajaperumal (1992). The ROSAT and EXOSAT flux densities agree in the overlapping region near 2 keV. We have performed a power-law fit to the joint ROSAT PSPC/EXOSAT ME data using the longest (Dec. 1983) EXOSAT observation (Fig. 3). The best-fit parameters (Table 8) are consistent with those for separate fits to the ROSAT and EXOSAT data.

6. Summary of X-ray variability for sample sources

X-ray variability is observed in four of the sample members: 0212+735, 0716+714, 0836+710, and 1928+738. No significant changes in spectral index are found for 0836+710, and 1928+738; for 1928+738 an unbroken power-law may extend from 0.2 keV to 10 keV. The spectral-slope difference for 0716+714 (between all ROSAT observations and the IPC measurement) may be consistent with curvature rather than requiring a variable spectral index. However, 0212+735 does exhibit a change in (IPC) spectral index over nine months; the spectrum in the second of the two observations is unusually hard and agrees with ROSAT measurements 10 years later.

0716+714 is the source with the fastest observed flux variability. The strength of the source assists in this detection. The variability is measured within the 20 ks ROSAT pointed observation, between the RASS and ROSAT pointed observations, and between the IPC and ROSAT pointed observations.

The X-ray variable sources 0716+714 and 0836+710 are the only two sources in our sample for which gamma-ray detections

Table 8. EXOSAT observations of 1928+738

observation date	livetime ks	N_H $[10^{20} cm^{-2}]^a$	1 keV flux density μJy^a	power-law energy index^a	red. χ^2 (dof)
		LE + ME, N_H fixed			
Oct 10, '83	12.4	7.4	$1.02^{+0.17}_{-0.16}$	$0.82^{+0.13}_{-0.13}$	1.01 (31)
Nov 12, '83	12.6	7.4	$0.74^{+0.13}_{-0.14}$	$1.00^{+0.30}_{-0.30}$	0.72 (34)
Dec 10, '83	30.4	7.4	$1.03^{+0.14}_{-0.13}$	$0.85^{+0.12}_{-0.12}$	0.83 (25)
Jan 10, '84	15.3	7.4	$0.80^{+0.13}_{-0.13}$	$1.32^{+0.25}_{-0.25}$	1.50 (25)
		ROSAT PSPC + EXOSAT ME, N_H free			
Dec 10, '84	30.4	$9.1^{+2.2}_{-1.7}$	$1.1^{+0.2}_{-0.2}$	$0.98^{+0.18}_{-0.18}$	0.70 (12)

[a] $\chi^2 + 2.3$ for fixed N_H fits; $\chi^2 + 3.53$ for free N_H fits.

are so far claimed with the EGRET detector on the *Compton* Observatory (Michelson et al. 1992; Fichtel et al. 1993).

7. Mean X-ray spectra

We have applied a maximum-likelihood method to determine the mean (α_{mean}) and width (σ_G) of the distribution of power-law spectral indices in our sample from the ROSAT data (Fig. 2), assuming that the underlying population exhibits a Gaussian distribution (see Worrall 1989 for a description of the method). We have made the approximation that the measurement error on the spectral index for each source is normally distributed (Fig. 1 and Table 5 show that this is a reasonable assumption for most sources in the sample), and we have used the average of the upper and lower errors given in Table 5.

In Figures 4 and 5 we present 68 % joint-confidence contours ($\{-2 \ln L\}_{min} + 2.3$) for α_{mean} and σ_G assuming the only absorption for each source is represented by its Galactic column-density of N_H. The mean power-law index is different for the quasars ($\alpha_{mean} = 0.59^{+0.17}_{-0.19}$) and the BL Lac objects ($\alpha_{mean} = 1.36^{+0.23}_{-0.27}$). 0716+714, due to its large number of counts (see Table 2), statistically dominates the BL Lac sample; removing it moves the result for the BL Lac objects to $\alpha_{mean} = 1.17^{+0.21}_{-0.27}$ which still differs from the mean for the quasars. Removing 0836+710, which statistically dominates the quasars, has a negligible effect on their mean spectral index which becomes $\alpha_{mean} = 0.62^{+0.23}_{-0.27}$. The removal of these two dominant sources does not alter the result of a different mean spectral index for the quasars and BL Lac objects.

We have tested whether the mean quasar and BL Lac X-ray spectral indices change when individual spectral fits allow the amount of absorption to vary. Although the results are less constrained due to the additional free parameter, the mean spectral indices from free N_H fits are consistent with the fixed N_H results. Both the fixed and free N_H results show that the distributions of power-law indices for the quasars and for the BL Lacs are *inconsistent* with a δ function distribution at the 90 % confidence level. Figures 4 and 5 demonstrate this for the case of fixed N_H.

The spectral indices measured for the five BL Lac objects in our sample separate into a group of three sources with $\alpha_x < 1.0$

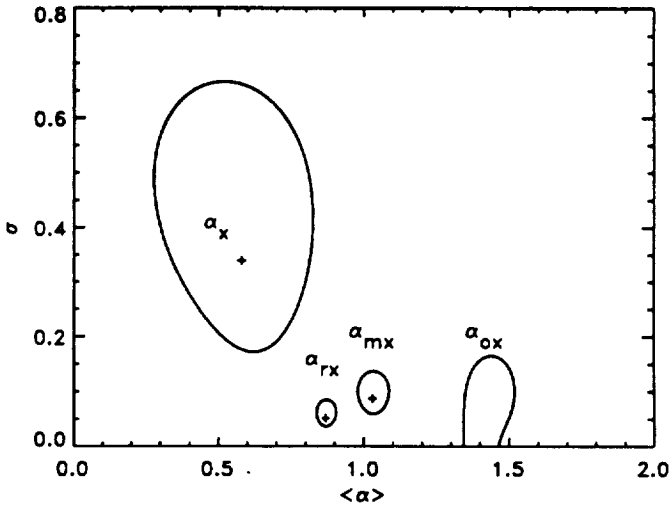

Fig. 4. Maximum likelihood contours for quasar subsample (68 % confidence contours for two parameters of interest). See sections 7 and 8.

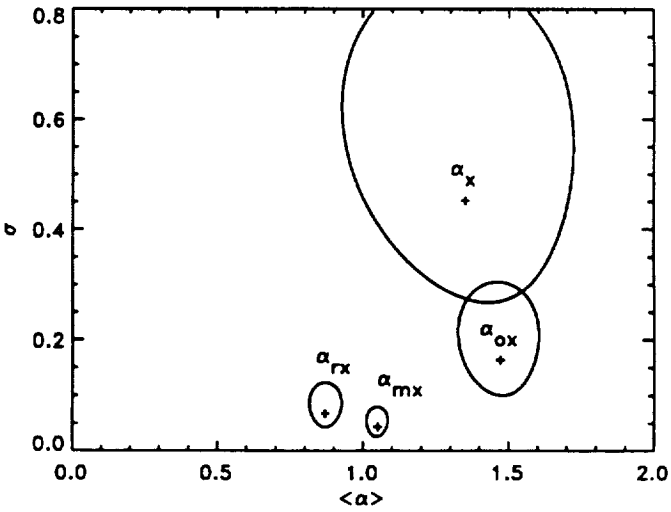

Fig. 5. Maximum likelihood contours for BL Lac subsample (68 % confidence contours for two parameters of interest). See sections 7 and 8.

and two sources with $\alpha_x > 1.7$, suggesting that these two groups may be members of different populations of BL Lac objects. The two low-redshift sources ($z < 0.35$) both have hard spectra while of the two sources with known high redshifts ($z > 0.65$) one displays a hard and the other a soft spectrum. 0716+714, the sample member for which the softest spectrum was measured, unfortunately does not have a measured redshift and therefore cannot be assigned unambiguously to either redshift group. With the available data it is premature to study any correlations of the power-law indices with other properties, such as redshift; a larger sample is needed.

8. Broad-band spectra

We have determined the radio to X-ray broad-band spectra for all targets using the ROSAT data and published radio to UV data. Table 9 gives flux densities used in our broad-band spectra. Radio and mm fluxes were taken from Kühr et al. (1981) and Steppe et al. (1988, 1992), respectively. The mean was taken where more than one flux measurement was available. We have used the optical magnitudes given in Véron-Cetty and Véron (1991) and have converted them to luminosity densities following Zamorani et al. (1981) and Marshall et al. (1983), and applying corrections for reddening following Seaton (1979). We calculate isotropic source-frame luminosity densities using the redshifts given in Table 1 and assuming a Friedmann cosmological model with $H_0 = 50$ km s^{-1} Mpc^{-1} and $q_0 = 0$. We have assumed $z = 0.5$ for the BL Lac object 0716 + 714 which has no measured redshift. This value for z is consistent with the lower-limit suggested for the source (Wagner 1993) and similar to the mean for the other BL Lac objects in our sample.

Fig. 6 shows luminosity densities; data are plotted at source-frame frequencies $\nu = \nu_{obs}/(1 + z)$. The broad-band spectral indices were calculated by interpolating the curves at 5 GHz, 230 GHz, 2500 Å and 2 keV. Since the data poorly define the spectral slope at 2500 Å, slopes of 0.5 for the quasars and 1.0 for the BL Lac objects were assumed.

We present the mean broad-band spectral properties of the quasars and BL Lac objects as maximum-likelihood confidence contours of the mean and width of the distribution of the three broad-band power-law indices α_{rx}, α_{mx}, α_{ox} (Figs. 4 and 5) and as histograms of the $\log \nu l_\nu - \log \nu_x l_x$ distribution, where ν is defined at the frequencies given above (Fig. 7). The mean broad-band spectral indices of the quasar and BL Lac samples are listed in Table 10. Note that likely errors due to the fact that the broad-band flux measurements used are non-contemporaneous with our X-ray observations are smaller or comparable in magnitude to the statistical errors of the broad-band indices. For example, 50 % flux variability in any of the spectral bands leads to an uncertainty of 0.02, 0.03 or 0.06 in the broad-band spectral indices α_{rx}, α_{mx}, and α_{ox}, respectively.

From a comparison of Figs. 4 and 5, the quasars and BL Lac objects in the sample do not differ in their mean values of α_{rx}, α_{mx} and α_{ox}. This is in contrast to Padovani (1992) who claims different mean α_{rx} values at the 96% confidence level for a flat radio spectrum quasar sample and a BL Lac sample.

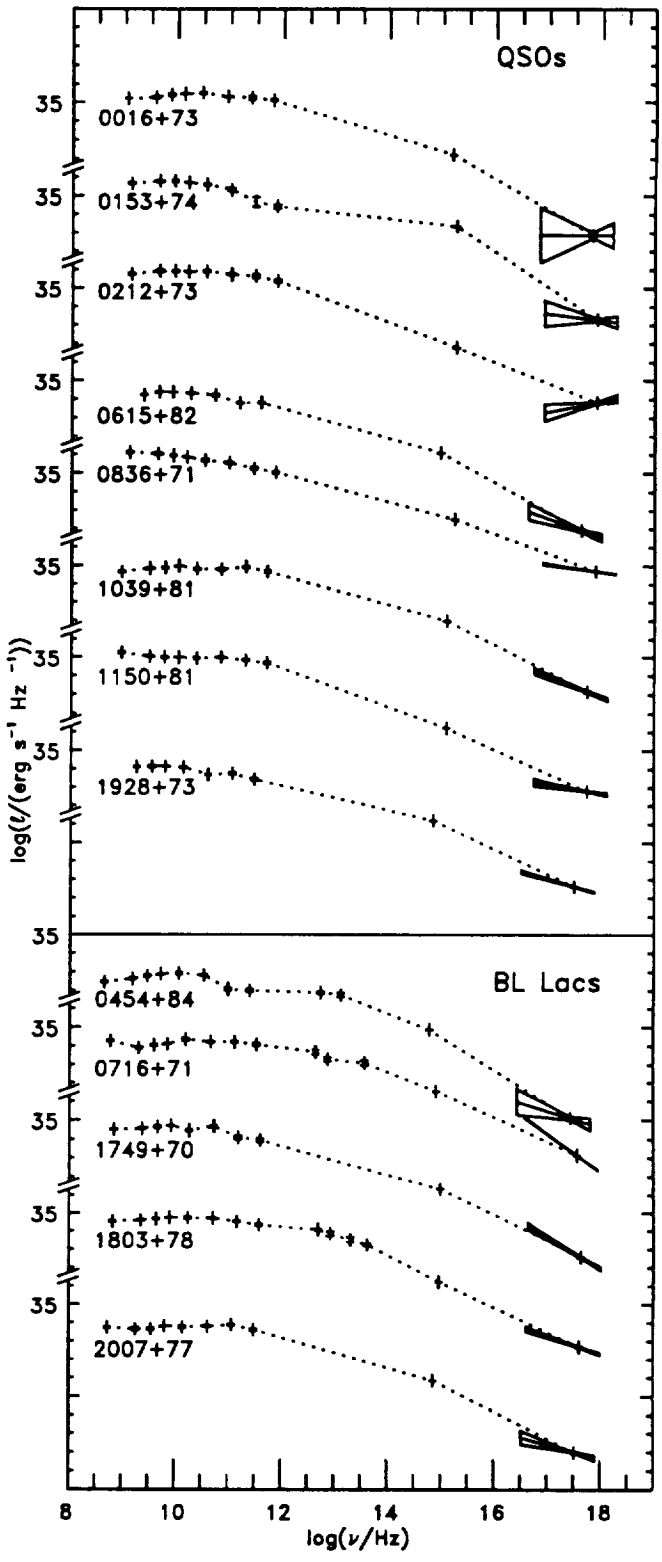

Fig. 6. Broad-band spectra. One tick mark on the luminosity scale represents one order of magnitude. The dashed lines were plotted to guide the eye and do not represent the true continuum. The luminosity points are non-contemporaneous and the spectra may be distorted due to variability. Flux measurements were taken from Kühr et al. (1981), Steppe et al. (1988 and 1992), Impey and Neugebauer (1988) and Véron-Cetty and Véron (1991).

Table 9. Broad-band flux-densities and spectral indices (see text for references)

target	1.4	2.7	5	90	230 GHz	m_V	α_{rx}^a	α_{mx}^a	α_{ox}^a	α_x^b
			[Jy]					1σ errors		
Quasars										
0016+731	1.06	1.50	1.65	1.01	0.73	18.0	0.927 ± 0.021	1.168 ± 0.029	1.674 ± 0.099	0.00 ± 1.34
0153+744	1.82	1.84	1.52	1.39	0.08	16.0	0.896 ± 0.013	0.958 ± 0.043	1.832 ± 0.084	0.35 ± 0.62
0212+735	2.38	2.37	2.20	1.29	0.69	20.0	0.902 ± 0.009	1.111 ± 0.016	1.210 ± 0.080	-0.56 ± 0.39
0615+820	0.69	1.02	1.00	0.26	0.27	17.5	0.940 ± 0.0011	1.095 ± 0.013	1.605 ± 0.083	1.02 ± 0.37
0836+710	3.90	3.16	2.59	0.62	0.39	16.5	0.780 ± 0.006	0.869 ± 0.011	1.074 ± 0.077	0.41 ± 0.03
1039+811	0.82	0.89	1.14	0.99	0.57	15.5	0.824 ± 0.007	1.049 ± 0.009	1.439 ± 0.078	1.09 ± 0.12
1150+812	1.40	1.25	1.22	0.87	0.61	18.5	0.893 ± 0.007	1.102 ± 0.009	1.284 ± 0.078	0.47 ± 0.17
1928+738	3.16	3.35	3.34	1.37	0.66	15.5	0.831 ± 0.006	0.953 ± 0.010	1.377 ± 0.077	0.80 ± 0.08
BL Lacs										
0454+844	0.77	1.11	1.39	0.22	0.18	16.5	0.997 ± 0.014	1.124 ± 0.020	1.799 ± 0.087	0.87 ± 0.59
0716+714	0.68	0.98	1.12	1.46	1.05	15.5	0.768 ± 0.006	0.983 ± 0.009	1.326 ± 0.077	2.01 ± 0.02
1749+701	1.25	1.57	1.81	0.43	0.32	17.0	0.892 ± 0.008	1.024 ± 0.015	1.415 ± 0.079	1.69 ± 0.13
1803+784	1.87	2.24	2.62	1.59	1.03	17.0	0.885 ± 0.007	1.081 ± 0.008	1.345 ± 0.078	0.97 ± 0.11
2007+777	0.85	0.83	1.26	1.46	0.78	16.7	0.858 ± 0.006	1.079 ± 0.010	1.446 ± 0.075	0.80 ± 0.33

[a] Broad-band index errors were determined from the published radio and mm 1σ errors. An error of 0.5 was assumed for the visual magnitudes (see text for details on how magnitudes were converted to luminosity densities).

[b] Symmetrical 1 σ errors, as required in our ML analysis (see sections 7 through 9), were determined by averaging the + and − errors given in Table 5.

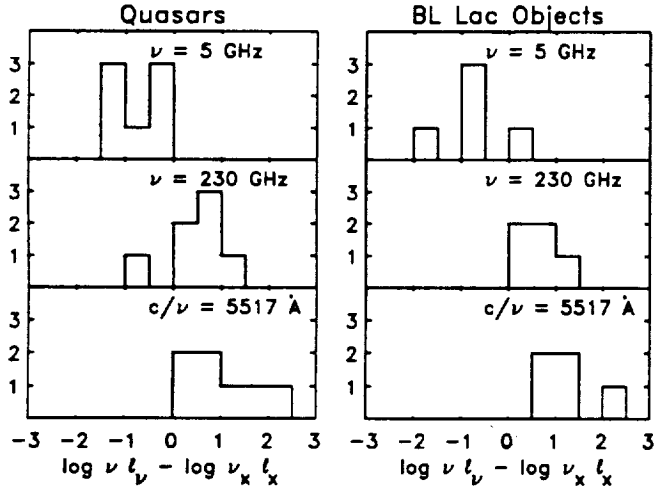

Fig. 7. Histograms of $\log \nu l_\nu - \log \nu_x l_x$ distribution for quasars (left) and BL Lac objects (right); ν taken at ν_r = 5 GHz, ν_{mm} = 230 GHz, and c/ν_o = 5517 Å(source frame).

The Padovani investigation is based on IPC data for 27 quasars ($f_{2.7\mathrm{GHz}} > 2$ Jy) as selected by Padovani and Urry (1992) from a flux-limited sample of Wall and Peacock (1985), and 28 BL Lac objects from the Stickel et al. (1991) 1 Jy sample. All of our BL Lac objects and 3 of our quasars are included. The slightly higher mean α_{rx} (0.89 ± 0.02) found by Padovani (1992) for the quasars is presumably due to the different selection criteria. Their result for the BL Lacs is slightly lower than our result but still within statistical agreement.

We have also studied the relationship of the X-ray power-law indices with α_{ox} on a source by source basis. We find that in the case of the BL Lac objects, $< \alpha_{ox} - \alpha_x >$ is consistent with 0. The distribution is relatively wide ($\sigma \sim 0.5$) implying that a fraction of the BL Lac objects have X-ray power-law indices which are either considerably steeper or considerably flatter than α_{ox} (see Fig. 8). As indicated in the previous section, the large dispersion may result from the superposition of two populations of BL Lac objects with different X-ray characteristics.

In the case of the quasars, the dispersion in $\alpha_{ox} - \alpha_x$ is relatively narrow and it is consistent with a δ function. The mean is given by $< \alpha_{ox} - \alpha_x >= 0.6$ (Fig. 8).

Table 10. Mean broad-band spectral indices

	α_{rx} [a]	α_{mx} [a]	α_{ox} [a]	α_x [a]
Quasars	0.88 ± 0.02	1.04 ± 0.03	1.41 ± 0.09	$0.59^{+0.17}_{-0.19}$
BL Lac objects	0.88 ± 0.03	1.06 ± 0.02	1.48 ± 0.07	$1.36^{+0.23}_{-0.27}$

[a] 68 % errors for one parameter of interest.

9. Comparison of X-ray and broad-band spectra with other samples

We find the mean X-ray spectrum for the quasars to be flatter than that for the BL Lac objects. This confirms earlier results by Worrall and Wilkes (1990) from an heterogenous sample of 31 flat radio spectrum quasars and 24 radio selected BL Lacs observed with the *Einstein* Observatory IPC.

For quasars, we find a hardening of the ROSAT spectrum as compared with α_{ox}, again confirming Worrall and Wilkes

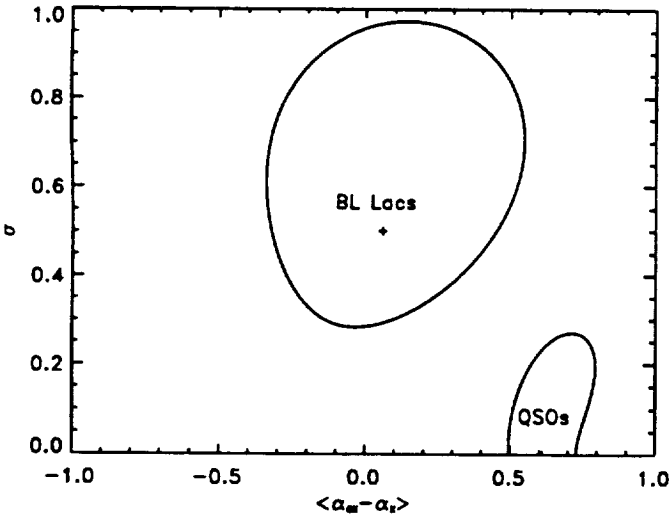

Fig. 8. Distribution of $\alpha_{ox} - \alpha_x$ for quasars and BL Lac objects.

(1990). Our result deviates from Worrall and Wilkes (1990) and from Lawson et al. (1992), who used the IPC and EXOSAT, respectively, in that we find that the quasar sample is *inconsistent* with a δ function distribution of power-law indices when N_H is left free to vary. The inconsistency may in part be driven by the spectra of 0836+71 and 1928+73 being different from one another; neither source was among those studies by the other authors. The dispersion we find may also be influenced by the softer response of ROSAT as compared with the IPC and EXOSAT.

In the BL Lac sample, our results differ from Worrall and Wilkes (1990) in that the mean X-ray power-law index is consistent with α_{ox}, and we see no large difference between the mean power-law indices determined from the free N_H and fixed N_H spectral fits. Since Worrall and Wilkes found the distribution of α_x to be flatter, on average, than α_{ox}, the two results taken together may suggest spectral curvature with the spectra flattening to higher energies. However, the large dispersion that we find in α_x requires the comparison of spectral index between lower and higher energies to be made on a source by source basis.

We find that the mean spectral index of the BL Lac objects in our radio-selected sample agrees with the mean from a heterogeneous sample of 10 X-ray-bright BL Lac objects observed in the RASS ($\alpha_{mean} \sim 1.4$; Fink et al. 1992). One of the sources, 1749+701, is in both samples. The Fink et al. sample comprises both X-ray-selected and radio-selected sources. Worrall and Wilkes (1990) have reported previously that X-ray bright radio-selected and X-ray-selected BL Lac objects display similar mean spectral indices in the *Einstein* Observatory IPC energy band.

The mean power-law spectral index of our quasars differs from that for X-ray bright quasars measured in the RASS (Brunner et al. 1992; Brinkmann et al. 1993). Unlike results presented here, the RASS flat radio spectrum quasar samples give a relatively steep spectral index ($< \alpha_x >= 1.13^{+0.2}_{-0.15}$; 68% confidence; Brunner et al. 1992). Two factors could contribute to the difference: (1) The luminosity and redshift range of the quasars differ. (2) The X-ray selected RASS sample favours soft, low N_H objects. Note that the mean Galactic N_H of the radio-selected sample reported here is relatively high ($\sim 1 \times 10^{21}$ cm^{-2}). In addition, the mean redshift is relatively high ($< z >\sim 1.6$), implying that any steep soft X-ray component will be shifted out of the ROSAT window. Brunner et al. (1992) find that the high-redshift ($1 < z < 3$) sub-group of the RASS quasars fits $< \alpha_x >= 0.5$, consistent with results presented here.

The mean redshift of the RASS quasars ($z \sim 0.7$) matches that of the BL Lac objects in our sample ($z \sim 0.6$), and the mean power-law indices are in reasonable agreement. This might suggest that redshift is at least as important as object class in determining the X-ray spectral index in the ROSAT band.

10. Synchrotron self-Compton models

The nonthermal broad band continuum of radio-loud quasars and BL Lac objects is most often discussed in the context of the synchrotron self-Compton (SSC) model. Below we present a short discussion of the broad band and new ROSAT data in the context of both symmetric and inhomogeneous SSC models.

10.1. Symmetric SSC models

Table 11 gives the transverse velocity, μ, for each source as measured with VLBI and taken from published work, and the inferred apparent velocity with respect to the velocity of light, β_{app} for two sets of cosmological parameters. Also given are the minimum Lorentz gamma, γ_{min}, and the corresponding angle to the line of sight, $i(\gamma_{min})$, and bulk relativistic Doppler factor, $\delta(\gamma_{min})$, corresponding to γ_{min}.

We have calculated the self-Compton emission at 1 keV using published radio data and the equations of Marscher (1983), and have compared it with the measured 1 keV X-ray emission from the current work to derive a minimum value for δ (Table 12). The radio core component of highest brightness temperature from Eckart et al. (1987) has been used, assuming an optically-thin spectral index of slope 0.7 extending to 10^{13} eV. For most sources we find δ_{min} is small, of order of or less than unity.

Eckart et al. (1986) speculated that for flat-spectrum objects such as these S5 sources, the radio brightness temperature may stay constant up to 300 GHz. This would lead to an increase in δ_{min} by roughly a factor of 3.6, and is the primary explanation of the larger values given by Schalinski (1990) and Schalinski et al. (1988; 1992a) who conclude that $\delta_{min} \sim \delta(\gamma_{min})$ (for $H_o = 100$ km s^{-1} Mpc^{-1}, $q_o = 0.5$) and that $i(\gamma_{min})$ is the upper limit to the angle of the radio jet to the line of sight.

From Tables 11 and 12, we conclude that since δ_{min} is small ($<< \delta[\gamma_{min}]$), one or more of the following conditions hold:

1. δ_{min} has been underestimated. This could be true because either the source sizes, θ, are smaller than the upper limits (a factor of $\sim 2 - 4$ [dependent on H_o] is required for $\delta_{min} \simeq \delta[\gamma_{min}]$), or there are higher-frequency radio components of

Table 11. Minimum Lorentz Gamma from Transverse Velocity Data

					$H_o = 100$ km s^{-1} Mpc^{-1}, $q_o = 0.5$				$H_o = 50$ km s^{-1} Mpc^{-1}, $q_o = 0$			
source	z	μ (mas/yr)	ref	notes	β_{app}	γ_{min}	$i(\gamma_{min})$	$\delta(\gamma_{min})$	β_{app}	γ_{min}	$i(\gamma_{min})$	$\delta(\gamma_{min})$
Quasars												
0016+731	1.781	0.22 ± 0.05	1		8.3	8.4	6.8°	8.4	25	25	2.3°	25
0153+744	2.338	< 0.022	2		≤ 0.9	-	-	-	≤ 3.2	-	-	-
0212+735	2.367	0.05 ± 0.03	3		2.2	2.4	25°	2.4	7.3	7.4	7.8°	7.4
0615+820	0.71	< 0.1	1,3,4		≤ 2.2	-	-	-	≤ 5.3	-	-	-
0836+710	2.17	0.13 ± 0.08	3,5	a	5.4	5.5	10°	5.5	17.6	17.6	3.3°	17.6
1039+811	1.26	< 0.07	1		≤ 2.2	-	-	-	≤ 6.0	-	-	-
1150+812	1.25	0.11 ± 0.05	3,4		3.5	3.6	16°	3.6	9.4	9.5	6.0°	9.5
1928+738	0.302	0.34 ± 0.05	6,7	a	4.0	4.1	14°	4.1	8.6	8.7	6.6°	8.7
BL Lacs												
0454+844	0.112	0.14 ± 0.04	3,4		0.7	1.2	56°	1.2	1.4	1.7	35°	1.7
0716+714	> 0.3	< 0.2	3,4	b	-	-	-	-	-	-	-	-
1749+701	0.77	0.26 ± 0.03	1,3	a	6.1	6.2	9.3°	6.2	14.9	14.9	3.8°	14.9
1803+784	0.6797	0.14 ± 0.05	8	a	3.0	3.2	18°	3.2	7.2	7.3	7.9°	7.3
2007+777	0.342	0.18 ± 0.04	4		2.3	2.5	23°	2.5	5.1	5.2	11°	5.2

References:

1. Schalinski et al. 1992b
2. Wüllner, K.H. 1992
3. Schalinski 1990
4. Witzel et al. 1988
5. Hummel et al. 1992b
6. Hummel et al. 1992a
7. Schalinski et al. 1992a
8. Krichbaum et al. 1993

Notes:

a. Jet with components of different speeds. Velocity of inner-most region adopted.
b. Redshift uncertain.

Table 12. Minimum Bulk Relativistic Doppler Factor from X-ray Data and self-Compton Calculation

		Radio components[a]						
source	z	ν_m (GHz)	S_m (Jy)	θ (mas)	S_x (μJy)[b]	δ_{min}	$\gamma(\delta_{min}, \beta_{app})$[c]	$i(\delta_{min}, \beta_{app})$[c]
Quasars								
0016+731	1.781	5.0	1.25	< 0.5	0.043	2.3	17, 146	13°, 2.5°
0153+744	2.338	5.0	0.64	< 0.7	0.072	0.7	-	-
0212+735	2.367	10.7	1.87	< 0.3	0.20	2.6	2.4, 12	23°, 14°
0615+820	0.71	5.0	0.61	< 0.5	0.036	0.7	-	-
0836+710	2.17	5.0	1.4	0.6	1.74[d]	1.1	14, 156	20°, 6.5°
1039+811	1.26	1.7	0.57	< 1.6	0.19	0.4	-	-
1150+812	1.25	1.67	1.09	2.0	0.087	0.6	11, 75	31°, 12°
1928+738	0.302	5.0	1.55	< 0.8	1.06	0.3	28, 126	28°, 13°
BL Lacs								
0454+844	0.112	5.0	0.8	< 0.5	0.024	0.6	1.5, 2.8	97°, 64°
0716+714	> 0.3	5.0	0.65	< 0.5	1.30	0.3	-	-
1749+701	0.77	1.67	0.56	< 2.0	0.14	0.2	96, 556	19°, 7.7°
1803+784	0.6797	5.0	2.04	< 0.5	0.23	1.6	4.0, 17	29°, 15°
2007+777	0.342	5.0	1.22	< 0.5	0.20[d]	0.8	4.4, 17	43°, 22°

[a] Core component of highest brightness temperature taken from Eckart et al. (1987). Assumed optically-thin spectral slope of 0.7 extends to 10^{13} eV.

[b] Observed results from this paper.

[c] First value is for $H_o = 100$ km s^{-1} Mpc^{-1}, $q_o = 0.5$; second is for $H_o = 50$ km s^{-1} Mpc^{-1}, $q_o = 0$.

[d] Average from multiple ROSAT observations. Weak dependence of δ_{min} on S_x; $\delta_{min} \sim S_x^{-0.185}$.

comparable brightness temperature (as speculated by Eckart et al. 1986; see above).
2. The self-Compton component falls below the measured X-ray emission so that $\delta > \delta_{\min}$.
3. The sources are at large angles to the line of sight ($\simeq i[\delta_{\min}, \beta_{app}]$) with large Lorentz factors ($\simeq \gamma[\delta_{\min}, \beta_{app}]$)
4. Calculations using a homogeneous moving sphere are too simplistic and a model involving plasma flowing in a jet is required.

We can assess the implications of these conditions. (1) is plausible but requires further radio data, such as may be obtained with the VLBA. (2) has implications concerning the interpretation of the X-ray data. It is best supported by the objects for which α_x is similar to α_{ox} (predominantly BL Lac objects) where there is no evidence for an additional emission component which may be of self-Compton origin. (3) is contrary to expectations from unified models which interpret flat-spectrum core-dominated sources such as those of the present sample to be jets at small angles to the line of sight. In a 5 GHz flux-limited sample such as this we expect a bias towards small angles to the line of sight and greater boosting of the radio emission. While (4) may indeed be true to fit the complete radio spectral and variability data, Ghisellini et al. (1993) show that only for $\delta_{\text{sphere}} > 1.0$ is $\delta_{\text{jet}} > \delta_{\text{sphere}}$. Interpretations using such jet models are discussed briefly below and in more detail in a forthcoming paper.

10.2. Inhomogeneous SSC models

We have applied the inhomogeneous plasma jet models of Königl (1981) and Ghisellini et al. (1985) to the broad-band data and find that for many sources we can fit the radio to soft X-ray data with a synchrotron spectrum alone. For those sources (all quasars and a fraction of the BL Lac objects) where the ROSAT spectrum is harder than the optical to X-ray broad-band spectrum, an additional Compton component is required. In the Ghisellini et al. model the jet is assumed to have a parabolically shaped inner section and a conical outer section, as compared with the Königl model where only a conical jet is considered. Our calculations are a special case of the Ghisellini et al. model where the power-law indices for the dependence of magnetic field and electron density with radius are the same in the parabolic and the conical sections; this reduces the number of free parameters from 16 to 14. We demonstrate the difference in mean X-ray spectra of the quasars and BL Lac objects by presenting a sample spectral fit of the Ghisellini et al. (1985) model for the brightest quasar 0836+710 (Fig. 9) and the BL Lac object 1749+701 (Fig. 10). Note that the steep X-ray spectrum of 1749+701 can be modeled well by the energy-loss dominated part of the synchrotron emission from the inner, paraboloid, section of the jet whereas for 0836+710 an additional Compton component is required. The set of spectral parameters given in Table 13 is not unique and only represents an example for a set of plausible jet parameters satisfying the broad-band spectral data. The synchrotron and self-Compton components of the inner, paraboloid (dotted and dashed lines) and outer, conical (dot dashed and triple dot dashed lines) section of the jet are plotted separately. Note that in the case of 0836+710 only the inner, conical section of the jet is used to model the data. A full account of our SSC model fits to the S5 broad-band data will appear in a forthcoming paper.

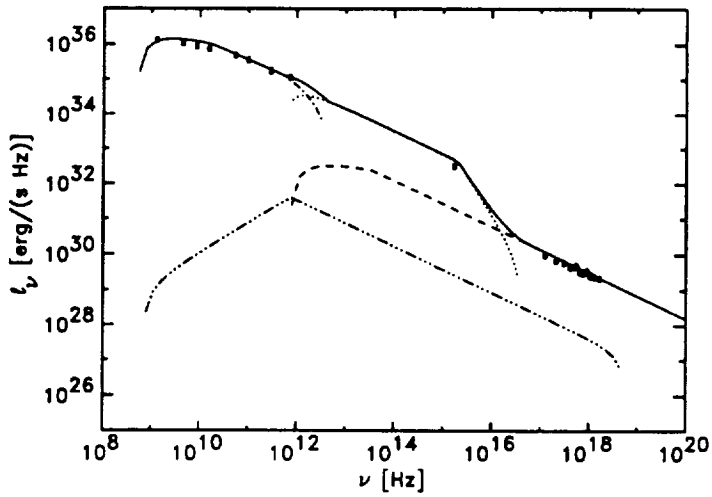

Fig. 9. Synchrotron-self-Compton model fit for 0836+710. The synchrotron and self-Compton components of the inner, paraboloid (dotted and dashed lines) and outer, conical (dot dashed and triple dot dashed lines) section of the jet are plotted separately.

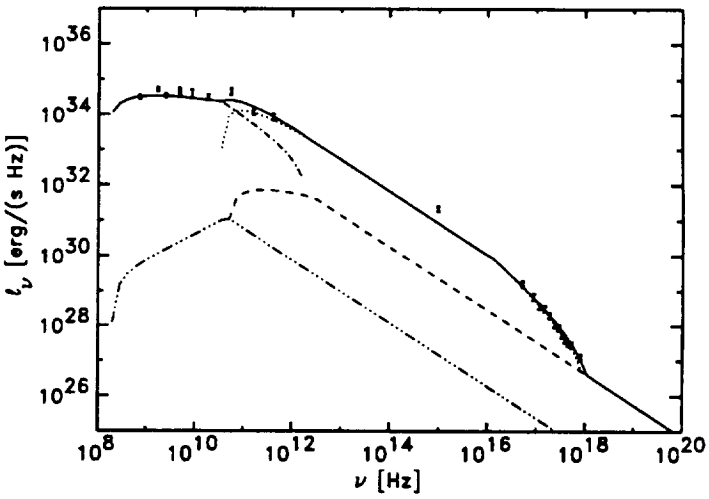

Fig. 10. Synchrotron-self-Compton model fit for 1749+701. (see Fig. 9 for an explanation of the curves)

11. Discussion

In our ROSAT PSPC observations of a complete flux limited sample of flat-spectrum (core-dominated) radio sources the mean power-law index of the 5 BL Lac objects is found to be

Table 13. Synchrotron-self-Compton model parameters

	S5 0836+710	S5 1749+701
$a[pc^{1-\epsilon}]$	4.5×10^7	4.5×10^7
ϵ	0.5	0.5
R_0 [pc]	3.6×10^{-5}	5.0×10^{-3}
R_1 [pc]	1.0	3.0
R_2 [pc]	1×10^4	1×10^4
Θ [rad]	0.1	0.03
B_0 [G]	15	25
K_0 [cm^{-3}]	1×10^9	4.5×10^6
α_0	0.65	0.9
m	0.6	1.0
n	2.1	1.8
γ_{max}	1×10^3	9×10^3
e	1.0	1.0
β	0.96	0.8
δ	6.3	3.0

a, ϵ: geometry parameters for parabolic section
R_0, R_1: inner and outer radii of jet (parabolic section)
R_1, R_2: inner and outer radii of jet (conical section)
Θ: inclination angle
B_0, K_0: B field and electron density at R_0
m, n: power-law index of radial B and K dependence
γ_{min}, γ_{max}: cutoff of electron distribution
e: power-law index for radial γ_{max} dependence
α_0: power-law index of electron energy distribution
β: v/c of bulk relativistic motion
δ: bulk relativistic Doppler factor (derived quantity)

considerably steeper ($\alpha_x \sim 1.3$) than that of the 8 quasars in the sample ($\alpha_x \sim 0.5$), confirming earlier results from the *Einstein* IPC. The relatively hard mean spectrum of our sample quasars (which have $< z > \sim 1.7$) is different from the mean power-law index of $\alpha_x \sim 1.1$ found for lower redshift RASS samples of flat radio spectrum quasars (which have $< z > \sim 0.7$). This may be explained by a break in the quasar spectra at low X-ray energies; the steeper low-energy component would be shifted out of the ROSAT PSPC response at higher redshifts and would not be visible with the *Einstein* IPC due to its higher mean energy response. A spectral break is also required to connect the hard X-ray spectrum to the broad-band continuum, indicated by the broad-band spectral index α_{ox}.

Although some of the difference in mean spectral index of our quasar and BL Lac samples may be attributed to the difference in mean redshifts (BL Lacs: $< z > \sim 0.7$), the relatively wide distribution of the BL Lac power-law indices does not appear to be matched by comparison samples of flat radio spectrum quasars at a similar mean redshift as observed in the RASS. If there is indeed a trend of BL Lac X-ray spectral index with redshift (section 7), it would be in the opposite sense from that for core-dominated quasars: BL Lacs and quasars appear to have different X-ray properties.

It is tempting to think of the wide dispersion of the X-ray spectral indices in our BL Lac sample as being due to the superposition of two physically distinct classes of objects. Different classes of BL Lac objects have recently been discussed by several authors (Kollgaard et al. 1992; Valtaoja et al. 1992; Impey et al. 1991). However, no obvious correlation between the X-ray spectral index and other source properties has been found so far and, clearly, a larger sample is needed to investigate this further.

In this context, it is also interesting to note that the distribution of the bulk relativistic Doppler factors δ for BL Lac objects has been claimed to be wider than the distribution for core-dominated quasars (Madau et al. 1987 and Ghisellini et al. 1993). In addition to the evidence from the X-ray spectra, this also suggests that BL Lac objects form a more diverse class of objects than the core dominated quasars. Unfortunately, due to its limited size, the sample investigated here does not permit a study of the shape of the δ distribution in detail.

The break indicated in the mean quasar X-ray spectrum from a comparison of our results with those from different samples observed in the RASS and with the *Einstein* IPC, may best be understood in terms of synchrotron self-Compton models, where the steep component is energy-loss-dominated synchrotron emission and the hard, high-energy component is once-scattered Compton emission.

Particularly in the case of quasars, steepening of the spectrum at low X-ray energies has also been widely discussed in the framework of thermal emission from an accretion disk (e.g., Czerny and Elvis 1987, Maraschi and Molendi 1990, Dörrer et al. 1992). Although this interpretation is more popular in the context of radio-quiet quasars, it has also been applied to at least one radio-loud quasar (3C 273; Turner et al. 1993), and Wandel and Urry (1991) have proposed an accretion disk model for BL Lac objects. In the soft X-ray range it may thus be necessary to disentangle the different contributions of a beamed, nonthermal broad-band component, most probably due to SSC emission from a jet, and thermal emission from an accretion disk.

We note that the brightest source in our sample, the quasar 0836+710, which also displays the hardest X-ray spectrum and which was found to vary by about a factor of two between our two ROSAT observations, has only recently been discovered in X-rays (*Einstein* slew survey, Elvis et al. 1992). Further study of this source, also known to be an emitter of γ rays, particularly at higher X-ray energies, seems highly desirable.

We are grateful to H. H. Fink for providing the RASS count rate spectrum of 1749+701, to A. Witzel, S. Wagner, Th. Krichbaum, R. Wegner and C. Hummel for helpful discussions, and to C. Lawrence for communication of redshifts in advance of publication. This research has made use of the NASA/IPAC Extragalactic Database which is operated by JPL, Caltech, under contract with NASA. DMW was supported by NASA grants NAG5-1724 and NAG5-1882.

References

Biermann, P.L., Duerbeck, H., Eckart, A. et al., 1981, ApJ, 247, L53
Biermann, P.L., Schaaf, R., Pietsch, W. et al., 1992, A&AS, 96, 339
Brinkmann, W., Siebert, J., Boller, Th., 1993, A&A, in press

Browne, I.W.A. and Murphy, D.W., 1987, MNRAS, 226, 601
Brunner, H., Worrall, D.M., Wilkes, B.J., Elvis, M., 1989, Proc. 23rd ESLAB Symp., eds. J. Hund and B. Battrick, ESA SP-296, p. 905
Brunner, H., Friedrich, P., Staubert, R. et al., 1991, in "Physics of Active Galactic Nuclei", eds. W.J. Duschl and S. J. Wagner, Springer-Verlag, Berlin, p. 77
Brunner, H., Friedrich, P., Zimmermann, H.-U., Staubert, R., 1992, in "X-ray emission from AGN and the cosmic X-ray background", eds. W. Brinkmann and J. Trümper, MPE report 235, 198
Canizares, C.R., White, J.L., 1989, ApJ, 339, 27
Chini, R., Steppe, H., Kreysa, E. et al., 1988, A&A, 192, L1
Comastri, A., Setti, G., Zamorani, G. et al., 1992, ApJ, 384, 62
Czerny, B., Elvis, M., 1987, ApJ, 321, 305
Dörrer, T., Friedrich, P., Brunner, H. et al., 1992, in "X-Ray emission from Active Galactic Nuclei and the Cosmic X-ray Background", eds. W. Brinkmann and J. Trümper, MPE Report 235, p. 130
Eckart, A., Witzel, A., Biermann, P.L. et al., 1986, A&A, 168, 17
Eckart, A., Witzel, A., Biermann, P.L. et al., 1987, A&AS, 67, 121
Elvis, M., Green, R.F., Bechtold, J. et al., 1986, ApJ, 310, 291
Elvis, M., Plummer, D., Schachter, J., et al., 1992, ApJS, 80, 257
Elvis, M., Fiore, F., Wilkes B.J., McDowell J.C., Bechtold, J., 1994, ApJ, in press (Feb. 10)
Fichtel, C.E., Bertsch, D.L., Hartman, R.C. et al., 1993, A&AS, 97, 13
Fink, H.H., Thomas, H.-C., Brinkmann, W., Okayasu, R., Hartner, G., 1992, in "X-ray emission from AGN and the cosmic X-ray background", eds. W. Brinkmann and J. Trümper, MPE report 235, 202
Ghisellini, G., Maraschi, L., and Treves, A., 1985, A&A, 146, 204
Ghisellini, G., Padovani, P., Celotti, A., and Maraschi, L., 1993, ApJ, 407, 65
Ghosh, K.K. and Soundararajaperumal, S., 1992, MNRAS, 254, 563
Grenier, I.A., Lebrun, F., Arnaud, M., Dame, T.M., Thaddeus, P., 1989, ApJ, 347, 231
Hasinger, G.G., 1993, private communication
Heeschen, D.S., Krichbaum, Th., Schalinski, C.J., and Witzel, A., 1987, AJ, 94, 1493
Heithausen, A. and Thaddeus, P., 1990, ApJ, 353, L49
Heithausen, A., Stacy, J.G., de Vries, H.W., Mebold, U., Thaddeus, P., 1993, A&A, 268, 265
Hewitt, A., Burbidge, G., 1987, ApJS, 63, 1
Hummel, C.A., Schalinski, C.J., Krichbaum, T.P., Witzel, A., and Johnston, K.J., 1988, A&A, 204, 68
Hummel, C.A., Schalinski, C.J., Krichbaum, T.P. et al., 1992a, A&A, 257, 489
Hummel, C.A., Muxlow, T.W.B., Krichbaum, T.P. et al., 1992b, A&A, 266, 93
Impey, C.D. and Neugebauer, G., 1988, AJ, 95, 307
Impey, C.D., Lawrence, C.R., Tapia, S., 1991, ApJ, 375, 46
Kembhavi, A., Feigelson, E.D., Singh, K.P., 1987, MNRAS, 220, 51
Kollgaard, R.I., Wardle, J.F.C., Roberts, D.H., Gabuzda, D.C., 1992, AJ, 104, 1687
Königl, A., 1981, ApJ, 243, 700
Krichbaum, T.P., 1992, private communication.
Krichbaum, T.P., Quirrenbach, A., and Witzel, A. 1992, in "Variability of Blazars", eds. E. Valtaoja and M. Valtonen (Cambridge University Press), p. 331
Krichbaum, T.P., Witzel, A., Graham, D.A., Schalinski, C.J., and Zensus, J.A., 1993, in "Sub-arcsecond Radio Astronomy", eds. R.J. Davies and R.S. Booth, (Cambridge: Cambridge University Press), p. 181
Kühr, H., Witzel, A., Pauliny-Toth, I.I.K., Nauber, U., 1981, A&AS, 45, 367
Lawrence, C.R., Pearson, T.J., Readhead, A.C.S., Unwin, S.,C. ,1986, AJ, 91, 494
Lawrence, C.R., 1992, private communication
Lawson, A.J., Turner, M.J.L., Williams, O.R. et al., 1992, MNRAS, 259, 743
von Linde, J., Borgeest, U., Schramm, K.-J. et al., 1993, A&A, 267, L23
Liszt, H.S. and Wilson, R.W., 1993, ApJ, 403, 663
Madau, P., Ghisellini, G., Persic, M., 1987, MNRAS, 224, 257
Maraschi, L., Molendi, S., 1990, ApJ, 353, 452
Marscher, A.P., 1983, ApJ, 264, 296
Marshall, H.L. et al, 1983, ApJ, 269, 42
Masnou, J.I., Wilkes, B.J., Elvis, M., McDowell, J.C., Arnaud, K.A., 1992, A&A, 253, 35
Michelson, P.F., Lin, Y.C., Nolan, P.L. et al., 1992, IAUC 5470
O'Dea et al., 1991, ApJ, 380, 66
Padovani, P., 1992, MNRAS, 257, 404
Padovani, P. and Urry, C.M., 1992, ApJ, 387, 449
Pearson, T.J. and Readhead, A.C.S., 1988, ApJ, 328, 114
Quirrenbach, A., Witzel, A., Wagner, S. et al., 1991, ApJ, 372, L71
Schalinski, C.J., Witzel, A., Krichbaum, Th.P, et al., 1988, IAU symposium 129, eds. M.J. Reid and J.M. Moran (Reidel), 71
Schalinski, C.J., 1990, Ph.D. Thesis, University of Bonn
Schalinski, C.J., Witzel, A., Hummel, C.A. et al., 1992a, in "Variability of Blazars", eds. E. Valtaoja and M. Valtonen, (Cambridge University Press), p. 221
Schalinski, C.J., Witzel, A., Krichbaum, T.P. et al., 1992b, "Variability of Blazars", ed E. Valtaoja and M. Valtonen, (Cambridge:Cambridge University Press), p. 225
Scoville, N.Z. and Sanders, D.B., 1987, "Interstellar Processes", eds. Hollenbach and Thronsen, (D. Reidel Publishing Company), p. 21
Seaton, M.J., 1979, MNRAS, 187, 73
Stark, A.A., Gammie, C.F., Wilson, R.W. et al., 1992, ApJS, 79, 77
Steppe, H., Salter, C.J., Chini, R. et al., 1988, A&AS, 75, 317
Steppe, H., Liechti, S., Mauersberger, R. et al., 1992, A&AS, 96, 441
Stickel, M., Fried, J.W., Kühr, H., 1989, A&AS, 80, 103
Stickel, M., Padovani, P., Urry, C.M., Fried, J.W., and Kühr, H., 1991, ApJ, 374, 431
Thompson, D.J., Bertsch, D.L., Dingus, B.L. et al., 1993, ApJ, 415, L13
Turner, M.J.L., Lawson, A.J., Saxton, R.D. et al., 1993, in preparation
Valtaoja, E., Teräsranta, H., Lainela, M., Terikorpi, P., 1992, in "Variability of Blazars", eds. E. Valtaoja and M. Valtonen, Cambridge University Press
Véron-Cetty, M.-P. and Véron, P., 1991, ESO Scientific Report No. 10
Voges, W., 1992, in "Space Science with particular emphasis on High Energy Astrophysics", Proceedings of "European International Space Year meeting", Munich
Wagner, S., Sanchez-Pons, F., Quirrenbach, A., Witzel, A., 1990, A&A, 235, L1
Wagner, S., Witzel, A., Heidt, J., et al., 1993, submitted to A&A
Wagner, S., 1993, private communication
Wagner, S., 1994, private communication
Wall, J.V., Peacock, J.A., 1985, MNRAS, 216, 173
Walter, R. and Fink, H.H., 1993, A&A, 274, 105
Wandel, A. and Urry, C.M., 1991, ApJ, 367, 78
Wegner, R. and Witzel, A., 1993, in "Sub-arcsecond radio astronomy", eds. R.J. Davis and R.S. Booth (Cambridge University Press), p. 165

Wilkes, B.J., Elvis, M., 1987, ApJ, 323, 243
Williams, O.R., Turner, T.L., Stewart, G.C. et al., 1992, ApJ, 389, 157
Witzel, A., Schalinski, C.J., Johnston, K.J. et al., 1988, A&A, 206, 245
Witzel, A., Wagner, S., Wegner, R., Steffen, W., Krichbaum, T., 1993, in "Sub-arcsecond radio astronomy", eds. R.J. Davis and R.S. Booth (Cambridge University Press), p. 159
Worrall, D.M., Giommi, P., Tananbaum, H., Zamorani, G., 1987, ApJ, 313, 596
Worrall, D.M., 1989, Proc. 23rd ESLAB Symp., ESP SP-296, 719
Worrall, D.M. and Wilkes, B.J., 1990, ApJ, 360, 396
Worrall, D.M., Conroy, M., DePonte, J. et al, 1992, in "Data Analysis in Astronomy IV", eds. V. Di Gesu et al., Plenum Press, p. 145.
Wüllner, K.H., 1992, Diploma Thesis, University of Bonn
Zamorani, G., Henry, J.P., Maccacaro, T. et al., 1981, ApJ, 245, 357
Zimmermann, H.-U., Belloni, T., Izzo, C., Kahabka, P., Schwentker, O., 1993, EXSAS Users Guide, 3rd edition, MPE Report 244, ISSN 0178-0719

This article was processed by the author using Springer-Verlag LaTeX A&A style file *L-AA* version 3.